(12)

NAVSWC TR 91-701

AD-A254 949

USE OF TARGET-ORIENTED PROCESS NOISE IN TRACKING MANEUVERING TARGETS

BY J. DARREN PARKER W. D. BLAIR
WEAPONS SYSTEMS DEPARTMENT

AUGUST 1992

Approved for public release; distribution is unlimited.

NAVAL SURFACE WARFARE CENTER
Dahlgren, Virginia 22448-5000 • Silver Spring, Maryland 20903-5000

USE OF TARGET-ORIENTED PROCESS NOISE IN TRACKING MANEUVERING TARGETS

BY J. DARREN PARKER W. D. BLAIR
WEAPONS SYSTEMS DEPARTMENT

AUGUST 1992

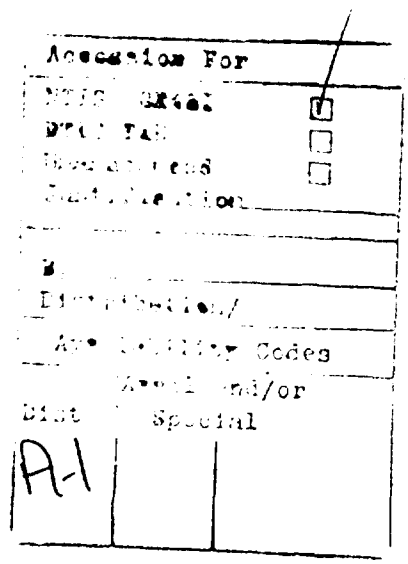

NAVAL SURFACE WARFARE CENTER
Dahlgren, Virginia 22448-5000 • Silver Spring, Maryland 20903-5000

FOREWORD

The reported research was conducted by Mr. J. Darren Parker NAVSWC (Code F21) and Mr. W. D. Blair NAVSWC (Code G71). The work described in this report was supported by the NAVSWC Independent Exploratory Development Program.

This document has been reviewed by K. M. Novell, Head, Weapons Direction Systems Branch.

Approved by:

DAVID S. MALYEVAC, Deputy Head
Weapons Systems Department

ABSTRACT

Kalman filters for target tracking typically use a process noise defined in the tracking frame. This requires setting the variances of the process noise in all three Cartesian coordinates to values large enough to compensate for the largest possible target maneuver. In general, the maneuvers performed by aircraft flying at high speeds are constant speed turns in a plane which are known as coordinated turns. An aircraft performs a coordinated turn by controlling its lateral acceleration which is approximately orthogonal to its velocity vector. Thus, it is logical that most of the uncertainty involved in tracking these targets is in the direction of the lateral acceleration. This information can be exploited by supplementing a standard Kalman filter with a target-oriented process noise. A target-oriented process noise is obtained by rotating a process noise, defined in the target's frame, into the tracking frame. The rotation matrix is computed from the state estimates of the Kalman filter.

The results of Monte Carlo simulations are presented which demonstrate that a Kalman filter with a target-oriented process noise tracks coordinated turning targets with smaller root-mean-square errors than a Kalman filter with standard process noise. It was determined that if the target-oriented process noise is to be effective, the Kalman filter must generate an acceleration estimate and the target's maneuver should be confined to a plane.

CONTENTS

Chapter		Page
1	INTRODUCTION	1-1
2	PROBLEM FORMULATION	2-1
	MODEL OF TARGET DYNAMICS	2-1
	MEASUREMENT MODEL	2-2
	KALMAN FILTER	2-4
3	TARGET MOTION MODELING	3-1
	CONSTANT VELOCITY	3-1
	CONSTANT ACCELERATION	3-2
	MEAN-JERK	3-2
4	TARGET-ORIENTED PROCESS NOISE	4-1
	REASONS FOR USING A TARGET-ORIENTED PROCESS NOISE	4-1
	PROCESS NOISE COVARIANCE IN TARGET'S FRAME	4-2
	ROTATION MATRIX	4-2
	KALMAN FILTER WITH TARGET-ORIENTED PROCESS NOISE	4-3
5	RESULTS	5-1
	TARGET TRAJECTORIES	5-1
	PARAMETER SELECTION	5-2
	SIMULATION RESULTS	5-4
6	CONCLUSIONS AND FUTURE RESEARCH	6-1
7	REFERENCES	7-1
	DISTRIBUTION	(1)

Appendix		Page
A	DERIVATION OF ROTATION MATRIX	A-1
B	ERROR ELLIPSE PLOTTING ALGORITHM	B-1

ILLUSTRATIONS

Figure		Page
5-1	TRAJECTORY 1	5-8
5-2	TRAJECTORY 2	5-9
5-3	TRAJECTORY 3	5-10
5-4	TRAJECTORY 4	5-12
5-5	RMS ERRORS FOR CV FILTER - TRAJ 1	5-13
5-6	RMS ERRORS FOR CA FILTER - TRAJ 2	5-14
5-7	RMS ERRORS FOR CA FILTER - TRAJ 3	5-15
5-8	RMS ERRORS FOR CA FILTER - TRAJ 4	5-16
5-9	RMS ERRORS FOR MJ FILTER - TRAJ 2	5-17
5-10	RMS ERRORS FOR MJ FILTER - TRAJ 3	5-18
5-11	RMS ERRORS FOR MJ FILTER - TRAJ 4	5-19
5-12	FILTERED ERROR COVARIANCES FOR CV FILTER - TRAJ 1	5-20
5-13	FILTERED ERROR COVARIANCES FOR CA FILTER - TRAJ 2	5-21
5-14	FILTERED ERROR COVARIANCES FOR CA FILTER - TRAJ 3	5-22
5-15	FILTERED ERROR COVARIANCES FOR CA FILTER - TRAJ 4	5-23
5-16	FILTERED ERROR COVARIANCES FOR MJ FILTER - TRAJ 2	5-24
5-17	FILTERED ERROR COVARIANCES FOR MJ FILTER - TRAJ 3	5-25
5-18	FILTERED ERROR COVARIANCES FOR MJ FILTER - TRAJ 4	5-26

ILLUSTRATIONS (continued)

Figure		Page
5-19	ROTATED PROCESS NOISE COVARIANCES FOR CV FILTER - TRAJ 1	5-27
5-20	ROTATED PROCESS NOISE COVARIANCES FOR CA FILTER - TRAJ 2	5-28
5-21	ROTATED PROCESS NOISE COVARIANCES FOR CA FILTER - TRAJ 3	5-29
5-22	ROTATED PROCESS NOISE COVARIANCES FOR CA FILTER - TRAJ 4	5-30
5-23	ROTATED PROCESS NOISE COVARIANCES FOR MJ FILTER - TRAJ 2	5-31
5-24	ROTATED PROCESS NOISE COVARIANCES FOR MJ FILTER - TRAJ 3	5-32
5-25	ROTATED PROCESS NOISE COVARIANCES FOR MJ FILTER - TRAJ 4	5-33
5-26	POSITION ERROR ELLIPSES FOR CV FILTER - TRAJ 1	5-34
5-27	POSITION ERROR ELLIPSES FOR CA FILTER - TRAJ 2	5-35
5-28	POSITION ERROR ELLIPSES FOR CA FILTER - TRAJ 3	5-36
5-29	POSITION ERROR ELLIPSES FOR CA FILTER - TRAJ 4	5-37
5-30	POSITION ERROR ELLIPSES FOR MJ FILTER - TRAJ 2	5-38
5-31	POSITION ERROR ELLIPSES FOR MJ FILTER - TRAJ 3	5-39
5-32	POSITION ERROR ELLIPSES FOR MJ FILTER - TRAJ 4	5-40

TABLES

Table		Page
5-1	STANDARD DEVIATION OF MEASUREMENT ERRORS	5-2
5-2	VARIANCES OF PROCESS NOISE FOR CV FILTER	5-3
5-3	VARIANCES OF PROCESS NOISE FOR CA FILTER	5-3
5-4	VARIANCES OF PROCESS NOISE FOR MJ FILTER	5-4

CHAPTER 1

INTRODUCTION

One of the more difficult targets to track is an aircraft flying at high speeds and performing maneuvers.[1-4] In general, the maneuvers performed by aircraft flying at high speeds are constant speed turns in a plane which are known as coordinated turns. An aircraft performs a coordinated turn by controlling its lateral acceleration which is approximately orthogonal to its velocity vector.[4-7] Thus, it is logical that most of the uncertainty involved in tracking these targets is in the direction of the lateral acceleration. This information can be exploited by supplementing a standard Kalman filter with a target-oriented process noise.

Most target tracking algorithms use a Kalman filter in which the uncertainty of the target's maneuvers is modeled with a process noise.[1,2] Since the process noise is usually defined in the tracking frame, the variances for each coordinate must be set high enough to account for the largest possible maneuver in each coordinate regardless of the target's orientation. This method imposes artificially high variances for the process noise because the uncertainty due to maneuvers must be equally distributed among the three coordinates.

A Kalman filter with a target-oriented process noise is obtained by defining the process noise in the target's frame and then rotating it into the tracking frame. By defining the process noise in the target's frame, the designer can set a high value for the variance of the lateral acceleration to account for the largest possible maneuver and lower values for the variances of the accelerations orthogonal to the lateral acceleration. Thus, using a target-oriented process noise provides the same tracking error through coordinated turns with a lower total acceleration error variance.

A Kalman filter with a target-oriented process noise designed to track coordinated turning targets is presented. The filter uses a rotation matrix to rotate a process noise defined in the target's frame into the tracking frame. The Kalman filter is implemented with three different motion models. The three motion models are constant velocity, constant acceleration, and mean-jerk which is a constant acceleration model with time-correlated jerks.

This report is organized as follows. In Chapter 2, the problem of target tracking is discussed. The techniques for modeling the motion of the targets are presented in Chapter 3. Chapter 4 explains the method used to implement a Kalman filter with a target-oriented process noise. Chapter 5 compares the performance of tracking filters using a target-oriented process noise are to that of tracking filters with a standard process noise. A summary and conclusions are given in Chapter 6, and the references are given in Chapter 7. Derivations of the rotation matrices are given in Appendix A, and an algorithm which can be used to generate error ellipses from filtered variances is presented in Appendix B.

CHAPTER 2

PROBLEM FORMULATION

The problem considered in this report is the tracking of a single target maneuvering through coordinated turns with no clutter or false measurements. In this chapter, the equations used to model the target dynamics and measurements are discussed. This chapter concludes with a presentation of the Kalman filter which is used for target tracking in this report.

MODEL OF TARGET DYNAMICS

The equation used to model the dynamics of a maneuvering target is given by

$$\dot{X} = f(X, u, w) \tag{2.1}$$

where X is the state vector, u is the target control vector, and w is the process noise vector representing possible deviations in $f(\cdot)$. The motion of the target is a continuous-time process as indicated by Equation (2.1), where $f(\cdot)$ is a dynamic constraint that defines the motion for the target in the form of a differential equation. The dynamic constraint, which is usually unknown to the tracking system, can differ significantly between targets and change for a common target during the tracking process.

The major problem with tracking maneuvering targets is that the control vector is not directly observable by the tracking system. When the target applies a control, a bias or lag develops in the estimates of the target state. The control can be included as acceleration in the dynamic constraint $f(\cdot)$, but the acceleration of coordinated turning targets usually varies with time in such a manner that a filter model cannot be clearly identified during tracking.

The target dynamics are usually modeled as linear in a Cartesian coordinate frame to simplify the filtering and reduce the computations required. Also, for convenience the continuous-time dynamics equation, Equation 2.1, is discretized. Thus, the equation used to model the target dynamics is given by

$$X_{k+1} = A_k X_k + B_k w_k \tag{2.2}$$

where $w_k \sim N(0, Q_k)$ is the process noise and A_k and B_k model the dynamics of the target. The Q_k is the covariance matrix of the process noise which is constant and diagonal for the Kalman filter with standard process noise but is dependent upon the orientation of the target for the Kalman filter with target-oriented process noise. The target state vector, X_k, may contain the position, velocity, and acceleration of the target at time k, as well as other variables used to model the time-varying acceleration. For a Kalman filter with standard process noise, the process noise covariance matrix is given by

$$Q_k = \begin{bmatrix} q_k^x & 0 & 0 \\ 0 & q_k^y & 0 \\ 0 & 0 & q_k^z \end{bmatrix} \tag{2.3}$$

where q_k^x, q_k^y, and q_k^z are the variances of the process noise in Cartesian coordinates. The q_k^x, q_k^y, and q_k^z are given the same value since the direction of the target control vector, u in Equation (2.1), is usually not observable.

MEASUREMENT MODEL

The equation used to model the measurements of the target's true state is

$$Z_k = h(X_k, v_k) \tag{2.4}$$

where Z_k is the discrete-time measurement vector at time k, and v_k is the measurement noise vector. As indicated by Equation (2.4), the measurement process is discrete-time because most sensors used for target tracking record the position and/or radial velocity at a given instant in time. In this report, the measurement process will be modeled as linear. Most sensors used for target tracking measure the target position in a spherical coordinate system, but the spherical measurements can be transformed into a Cartesian coordinate frame for processing as a linear function of the target state. The transformation from spherical to

Cartesian coordinates is given by

$$x = R\,\cos E\,\sin B \tag{2.5a}$$

$$y = R\,\cos E\,\cos B \tag{2.5b}$$

$$z = R\,\sin E \tag{2.5c}$$

where $R, B, and E$ are the range, bearing, and elevation, respectively. Thus, the linear measurement process is then given by

$$Z_k = H_k X_k + v_k \tag{2.6}$$

where Z_k is the target measurement in the Cartesian coordinate frame. The mean of the measurement noise, v_k, is $E[v_k] = 0$, and the covariance matrix of the measurement noise is $R_k = E[v_k v_k^T]$. The H_k is a vector which selects the states which correspond to the measurements and (in a single coordinate) is given by

$$H_k = [1 \quad 0 \quad 0 \quad 0] \tag{2.7}$$

for a 4 state model with measurements of position only. The H_k for a 3 state model is the first 3 elements of Equation (2.7) and the first 2 elements for a 2 state model.

The measurement errors in spherical coordinates are usually assumed to be white and Gaussian and uncorrelated in range, bearing, and elevation, but the transformation to the rectangular coordinate frame causes the components of v_k to become non-Gaussian and correlated. Nevertheless, for most probability calculations v_k is often assumed to be Gaussian. The correlation between the components of v_k can be modeled by linearizing the transformation from spherical to Cartesian coordinates of Equation (2.5) with a first-order Taylor series. Thus, the covariance matrix of the measurement noise, R_k, is computed from the equation

$$R_k = U \begin{bmatrix} \sigma_R^2 & 0 & 0 \\ 0 & \sigma_B^2 & 0 \\ 0 & 0 & \sigma_E^2 \end{bmatrix} U^T \tag{2.8}$$

where

$$U = \begin{bmatrix} \cos\bar{E}\,\sin\bar{B} & \bar{R}\,\cos\bar{E}\,\cos\bar{B} & -\bar{R}\,\sin\bar{E}\,\sin\bar{B} \\ \cos\bar{E}\,\cos\bar{B} & -\bar{R}\,\cos\bar{E}\,\sin\bar{B} & -\bar{R}\,\sin\bar{E}\,\cos\bar{B} \\ \sin\bar{E} & 0 & \bar{R}\cos\bar{E} \end{bmatrix} \tag{2.9}$$

and σ_R^2, σ_B^2, and σ_E^2 are the measurement error variances for range, bearing, and elevation, respectively. The $\bar{R}, \bar{B}, and \bar{E}$ are the estimated range, bearing, and elevation, respectively, which are computed from the state estimates at time k.

CHAPTER 3

TARGET MOTION MODELING

The three different motion models considered in this report are constant velocity, constant acceleration, and mean-jerk. The constant velocity and constant acceleration motion models are commonly used, but the mean-jerk motion model is relatively new. These three motion models are described in this chapter. For simplicity, the motion models are presented in the form that would be used to track in a single coordinate. The motion models used to track in three coordinates simultaneously are block diagonal matrices, with the A_k and B_k matrices presented in this chapter forming the blocks.

CONSTANT VELOCITY

The first model presented is constant velocity and, for a single coordinate, the motion model is given by

$$A_k = \begin{bmatrix} 1 & T \\ 0 & 1 \end{bmatrix} \tag{3.1}$$

$$B_k = \begin{bmatrix} 0.5T^2 & T \end{bmatrix}^T \tag{3.2}$$

where T is the time interval between measurement k and $k+1$. The elements of the state vector X_k are position and velocity. In this report, a Kalman filter using this motion model is referred to as a CV filter.

CONSTANT ACCELERATION

The second model is constant acceleration and, for a single coordinate, the motion model is given by

$$A_k = \begin{bmatrix} 1 & T & 0.5T^2 \\ 0 & 1 & T \\ 0 & 0 & 1 \end{bmatrix} \tag{3.3}$$

$$B_k = \begin{bmatrix} 0.5T^2 & T & 1 \end{bmatrix}^T \tag{3.4}$$

The elements of the state vector for this model are position, velocity, and acceleration. A Kalman filter using this motion model is referred to as a CA filter in this report.

MEAN-JERK

The third model is the mean-jerk model which is the standard constant acceleration model with time-correlated jerk. The use of the time-correlated jerk represents the fact that the acceleration changes in a deterministic manner as a target maneuvers. Thus, the jerk at time k will be related to those at time $k-1$ if the difference between these times is small. The continuous-time form of the mean-jerk model, in a single coordinate, is given by

$$\dot{X} = \begin{bmatrix} 0 & 1 & 0 & 0 \\ 0 & 0 & 1 & 0 \\ 0 & 0 & 0 & 1 \\ 0 & 0 & 0 & -\tau \end{bmatrix} X + \begin{bmatrix} 0 \\ 0 \\ 0 \\ 1 \end{bmatrix} w(t) \tag{3.5}$$

where

$$X = \begin{bmatrix} x & \dot{x} & \ddot{x} & x^j \end{bmatrix}^T \tag{3.6}$$

The variable, x^j, is the jerk which is the time derivative of the acceleration. The discrete-time form of the model is given by

$$A_k = \begin{bmatrix} 1 & T & 0.5T^2 & \tau^{-3}(0.5(\tau T)^2 - \tau T + 1 - e^{-\tau T}) \\ 0 & 1 & T & \tau^{-2}(e^{-\tau T} - 1 + \tau T)) \\ 0 & 0 & 1 & \tau^{-1}(1 - e^{-\tau T}) \\ 0 & 0 & 0 & e^{-\tau T} \end{bmatrix} \tag{3.7}$$

$$B_k = \begin{bmatrix} \tau^{-4}(\frac{1}{6}(\tau T)^3 - 0.5(\tau T)^2 + (\tau T - 1 + e^{-\tau T})) \\ \tau^{-3}(0.5(\tau T)^2 - \tau T + 1 - e^{-\tau T}) \\ \tau^{-2}(e^{-\tau T} - 1 + \tau T)) \\ \tau^{-1}(1 - e^{-\tau T}) \end{bmatrix} \tag{3.8}$$

and

$$X_k = \begin{bmatrix} x_k & \dot{x}_k & \ddot{x}_k & x_k^j \end{bmatrix}^T \tag{3.9}$$

The variable τ is related to the correlation of the jerk. In this report, τ was chosen to be 0.5 to give a 2 second time constant for the correlation. In the derivation of the discrete-time model, $w(t)$ in Equation (3.5) was assumed to be constant between times k and $k+1$. A Kalman filter using the motion model given by Equations (3.7) and (3.8) is referred to as a MJ filter in this report.

CHAPTER 4

TARGET-ORIENTED PROCESS NOISE

The method used to implement a Kalman filter with a target-oriented process noise is described in this chapter. First, the reasons for using a target-oriented process noise are discussed. Then, a process noise covariance matrix defined in the target's frame is presented. Next, the rotation matrices used to rotate the process noise defined in the target's frame into the tracking frame are presented. Finally, the Kalman filter with target-oriented process noise is presented.

REASONS FOR USING A TARGET-ORIENTED PROCESS NOISE

The Kalman filter with target-oriented process noise allows the designer to define the process noise covariance in terms of thrust and lateral accelerations. This allows the Kalman filter to more realistically model the maneuverability of the target. Most targets maneuver by controlling their thrust acceleration which is parallel to the target velocity vector, and/or their lateral acceleration which is orthogonal to the target velocity vector. Except for missiles in launch or boost phases, the thrust acceleration of most targets is limited to 10 m/s^2. However, the lateral acceleration can approach 150 m/s^2. Thus, when tracking a maneuvering target, a wider range of uncertainty exists due to the lateral acceleration than due to the thrust acceleration. For this reason, a Kalman filter with target-oriented process noise can model the acceleration uncertainty more accurately than a Kalman filter with standard process noise. This causes the error covariances of the state estimates, Equation (2.14) to have a smaller trace. Smaller error variances lead to smaller errors and smaller position error ellipsoids. Reducing the errors in the state estimates improves the performance of fire control systems, and reducing the volume of the position error ellipsoids improves the tracking of targets in a cluttered environment.

PROCESS NOISE COVARIANCE IN TARGET'S FRAME

The process noise covariance matrix defined in the target's frame is

$$Q_k^{tg} = \begin{bmatrix} q_k^t & 0 & 0 \\ 0 & q_k^l & 0 \\ 0 & 0 & q_k^{tl} \end{bmatrix} \tag{4.1}$$

where q_k^t is the variance of the thrust acceleration, q_k^l is the variance of the lateral acceleration, and q_k^{tl} is the variance of the acceleration orthogonal to both q_k^t and q_k^l. The target's frame is defined with the X axis aligned with the target's velocity vector, the Y axis aligned with the target's lateral acceleration vector, and the Z axis aligned with the cross product of the target's velocity and lateral acceleration vectors which forms a right-handed coordinate system. The value of q_k^l is determined in the exact same manner that q_k^x, q_k^y, and q_k^z are determined in a Kalman filter with standard process noise. The value of q_k^t is set to λq_k^l, where $0 < \lambda < 1$. This is done because the targets considered in this report are constant speed, so there is less uncertainty in the thrust acceleration as compared to the lateral acceleration. The value of q_k^{tl} is set to one of two values. For the CV filter, q_k^{tl} is set to q_k^l, and for the CA and MJ filters, q_k^{tl} is set to γq_k^l where $0 < \gamma < 0.01$. The variance, q_k^{tl}, is lowered for the CA and MJ filters because the targets considered in this report maneuver by performing coordinated turns. Since a coordinated turn is defined as a constant speed turn in a plane, there will be little acceleration uncertainty in the direction of q_k^{tl} which is orthogonal to this plane. This cannot be done in the CV filter because no acceleration estimate is calculated, so the plane defined by the velocity and lateral acceleration vectors cannot be determined. Thus, for the CV filter, there is equal acceleration uncertainty in the directions of q_k^l and q_k^{tl}.

ROTATION MATRIX

A target-oriented process noise requires a rotation matrix to rotate the process noise, defined in the target's frame, into the tracking frame. Two different rotation matrices are presented. A rotation matrix based on velocity and acceleration estimates is used for the CA and MJ filters, and a rotation matrix based on velocity estimates only is used for the CV filter. The rotation matrix used in the CA and MJ filters is

$$D_k = \begin{bmatrix} \dfrac{V_k}{|V_k|} & \dfrac{A_k^l}{|A_k^l|} & \dfrac{V_k \times A_k^l}{|V_k||A_k^l|} \end{bmatrix} \tag{4.2}$$

where $V_k = [\dot{x}_k \quad \dot{y}_k \quad \dot{z}_k]^T$ is the velocity vector of the target, $A_k^l = \left[\ddot{x}_k^l \quad \ddot{y}_k^l \quad \ddot{z}_k^l\right]^T$ is the lateral acceleration vector of the target, $|V_k|$ is the magnitude or length of V_k, and $V_k \times A_k^l$ is the cross product of V_k and A_k^l. The lateral acceleration vector, A_k^l, is computed by subtracting the thrust acceleration vector from the acceleration vector, A_k, using the equation[7]

$$A_k^l = A_k - \frac{(A_k \cdot V_k)}{|V_k|^2} V_k \tag{4.3}$$

The rotation matrix used for the CV filter is

$$D_k = \begin{bmatrix} \frac{\dot{x}_k}{S} & \frac{-\dot{y}_k}{Sh} & \frac{-\dot{x}_k\,\dot{z}_k}{S\,Sh} \\ \frac{\dot{y}_k}{S} & \frac{\dot{x}_k}{Sh} & \frac{-\dot{y}_k\,\dot{z}_k}{S\,Sh} \\ \frac{\dot{z}_k}{S} & 0 & \frac{Sh}{S} \end{bmatrix} \tag{4.4}$$

where $S = |V_k|$ and $Sh = (\dot{x}_k^2 + \dot{y}_k^2)^{\frac{1}{2}}$. The rotation matrix for the CV filter given by Equation (4.4) is derived in Appendix A from the rotation matrix for the CA and MJ filters given by Equation (4.2). Since the true state of the target cannot be determined during tracking, the filtered estimates of the target's state are used in Equations (4.2), (4.3), and (4.4).

KALMAN FILTER WITH TARGET-ORIENTED PROCESS NOISE

A Kalman filter with target-oriented process noise is obtained by rotating the process noise defined in the target's frame into the tracking frame. The target state model of Equation (2.2) then becomes

$$X_{k+1} = A_k X_k + B_k D_k w_k^{tg} \tag{4.5}$$

where w_k^{tg} is the process noise defined in the target's frame, and D_k is a rotation matrix given by either Equation (4.2) for the CA and MJ filters or Equation (4.4) for the CV filter. The only Kalman filter equations explicitly affected by the process noise are the time update equations, Equations (2.10) and (2.11). Since the process noise is considered to be zero mean in this report, Equation (2.10) is not affected by the rotation of the process noise. Equation (2.11) becomes

$$P_{k+1|k} = A_k P_{k|k} A_k^T + B_k Q_k^r B_k^T \tag{4.6}$$

where Q_k^r is the rotated process noise covariance given by

$$Q_k^r = \quad D_k Q_k^{tg} D_k^T \tag{4.7}$$

where D_k is the rotation matrix and Q_k^{tg} is the process noise covariance matrix defined in the target's frame given by Equation (4.1). Thus, to obtain a Kalman filter with target-oriented process noise, the standard Kalman filter given by Equations (2.10-14) are used except Equation (2.11) is replaced by Equation (4.6).

CHAPTER 5

RESULTS

Simulation results of Kalman filters with target-oriented process noise are compared with those of Kalman filters with standard process noise. Simulation results for Kalman filters with three different motion models are presented for four different target trajectories. The standard process noise filters and target-oriented process noise filters are compared on the basis of root-mean-square (RMS) errors, filtered error covariances, process noise covariances, and position error ellipses. All of the figures referred to in this chapter are located at the end of the chapter.

TARGET TRAJECTORIES

The four target trajectories used in the filter simulations are all constant speed with some type of coordinated turn. The speed used for all four trajectories was 300 m/s. One trajectory was used to generate the simulation results for the CV filters, and the other three trajectories were used to generate the simulation results for the CA and MJ filters. The trajectory used for the CV filters is a weave in the X-Y plane with a peak acceleration of 2.5 m/s^2 and a constant altitude of 1 km. This trajectory is referred to as Trajectory 1 in this report; Figure 5-1 illustrates this trajectory. The trajectories used for the CA and MJ filters are referred to as Trajectories 2, 3, and 4 in this report. Trajectory 2 is a weave in the X-Y plane with a peak acceleration of 30 m/s^2 and a constant altitude of 1 km. Trajectory 3 is a constant speed turn in a plane rotated 45 degrees about the X axis with a peak acceleration of 30 m/s^2 . Trajectory 4 is a constant speed turn in the X-Y plane with a peak acceleration of 30 m/s^2 and a constant altitude of 1 km. Figures 5-2, 5-3, and 5-4 illustrate these trajectories.

These trajectories were used to simulate radar measurements by adding white Gaussian noise to the true spherical coordinate trajectory (i.e. Range, Bearing, and Elevation). These simulated radar measurements were converted to Cartesian coordinates using Equations (2.5a,b,c). A new set of radar measurements was generated for each run of the Monte Carlo simulations.

PARAMETER SELECTION

The parameters that were the same for all of the simulation results were the data rate, the standard deviations of the measurement noise, the number of data points used to initialize the track, and the number of runs used for Monte Carlo simulations. The data rate was chosen to be 5 Hz. The standard deviations of the measurement noise were chosen to be 8 m in the range coordinate and 2 mrad in the bearing and elevation coordinates. The number of data points used to initialize the track was chosen to be 5. The number of runs used in the Monte Carlo simulations to compute the RMS errors was chosen to be 200.

The standard deviation of the measurement noise was estimated for each trajectory, so the process noise variances could be chosen. The measurement noise standard deviation was assumed to be

$$\sigma_m = \frac{\sigma_r + R_{max}\sigma_b + R_{max}\sigma_e}{3} \tag{5.1}$$

where the subscripts m, r, b, and e denote measurement, range, bearing, and elevation respectively, and R_{max} is the maximum range for the particular trajectory. The values calculated for σ_m for each trajectory are presented in Table 5-1.

TABLE 5-1. STANDARD DEVIATION OF MEASUREMENT ERRORS

Trajectory	1	2	3	4
Std Dev (m)	40.4	40.4	18.7	56.0

The process noise covariances matrices were the only other parameters required to perform the simulations. To simplify the discussions of the results, the Kalman filters with standard process noise are referred to as SPN filters, and the Kalman filters with target-oriented process noise are referred to as TOPN filters.

The SPN filters use the process noise covariance matrix given in Equation (2.3). The diagonal elements were chosen to be equal (i.e. $q_k^x = q_k^y = q_k^z = q_k$). The process noise variance, q_k, was calculated from the steady-state position gain, the variance of the measurement errors, and the time interval between measurements.[12] The steady-state position gain, α (the same variable used in an $\alpha - \beta$ filter), was chosen to be 0.3. The TOPN filters use the process noise covariance matrix given in Equation (4.1). The variances of the process noise for the TOPN filters were determined from the value of q_k for the corresponding SPN filter. For the CA and MJ TOPN filters, $q_k^t = q_k^l = q_k$ and $q_k^{tl} = 0.01 q_k$. For the CV TOPN filter, $q_k^l = q_k^{tl} = q_k$ and $q_k^t = q_k/4$. The values for these process noise variances for both the SPN and TOPN filters are presented in Tables 5-2, 5-3, and 5-4.

TABLE 5-2. VARIANCES OF PROCESS NOISE FOR CV FILTER

	q_k (m^2/s^4)	$q_k{}^t$ (m^2/s^4)	$q_k{}^l$ (m^2/s^4)	$q_k{}^{tl}$ (m^2/s^4)
Traj #1	4250	4250/4	4250	4250

TABLE 5-3. VARIANCES OF PROCESS NOISE FOR CA FILTER

	q_k (m^2/s^4)	$q_k{}^t$ (m^2/s^4)	$q_k{}^l$ (m^2/s^4)	$q_k{}^{tl}$ (m^2/s^4)
Traj #2	35	35	35	0.35
Traj #3	8	8	8	0.08
Traj #4	65	65	65	0.65

TABLE 5-4. VARIANCES OF PROCESS NOISE FOR MJ FILTER

	q_k (m^2/s^8)	q_k^t (m^2/s^8)	q_k^l (m^2/s^8)	q_k^{tl} (m^2/s^8)
Traj #2	270	270	270	2.7
Traj #3	58	58	58	0.58
Traj #4	518	518	518	5.18

SIMULATION RESULTS

The root-mean-square errors (RMSE), filtered error covariances, process noise covariances, and position error ellipses of Monte Carlo simulations for the SPN and TOPN filters are presented. The CV filters were simulated using trajectory 1 only. The CA and MJ filters were each simulated using trajectories 2, 3, and 4.

Root-Mean-Square Errors

The RMSE obtained from these simulations are shown in Figures 5-5 through 5-11. The RMSE were calculated by summing the squared filter errors from all runs, dividing by 200, and then taking the square root. The RMSE for the CV SPN and TOPN filters are shown in Figure 5-5. The position error was the same for both filters throughout the entire trajectory. The velocity error was slightly smaller for the TOPN filter. The RMSE for the CA SPN and TOPN filters are shown in Figures 5-6 through 5-8. The position, velocity, and acceleration errors were smaller for the TOPN filter for all three trajectories. However, of the three trajectories, the largest reduction in errors occurred for trajectory 4 as shown in Figures 5-8. Note that this is also the trajectory in which the range to the target is largest. The RMSE for the MJ SPN and TOPN filters are shown in Figures 5-7 through 5-11. The differences between the errors for these filters were similar to those of the CA SPN and TOPN filters.

Filtered Error Covariances

The filtered error covariances of the state estimates, given by Equation (2.14), from a single run of each filter are shown in Figures 5-12 though 5-18. These error covariances are the sum of the error covariances of all three coordinates. As Figure 5-12 shows, the filtered error covariances for the CV TOPN filter are slightly less than those for the CV SPN filter. As Figures 5-13 through 5-18 show, the filtered error covariances for the CA and MJ TOPN filters are significantly less than those for the CA and MJ SPN filters. Note that the filtered error covariances change slowly throughout the trajectories. This happens because the filtered error covariances are functions of the Kalman gain, K_k, which is a function of the measurement error covariance, R_k, and R_k depends on the estimated range to the target (see Equations (2.8), (2.9), (2.12), and (2.14)).

Process Noise Covariances

The rotated process noise covariance matrices for the TOPN filters from a single run of each filter are shown in Figures 5-19 through 5-25. In these figures, Qr denotes the rotated process noise covariance matrix given by Q_k^r in Equation (4.7). All six elements of Qr are plotted in each figure. The Qr(1,1), Qr(2,2), and Qr(3,3) are the diagonal elements of Qr which are the rotated process noise variances in the X, Y, and Z coordinates, respectively. The Qr(1,2) is the rotated process noise covariance between the X and Y coordinates. Likewise, Qr(1,3) is the rotated process noise covariance between the X and Z coordinates, and Qr(2,3) is the rotated process noise covariance between the Y and Z coordinates. The process noise covariance matrices for the SPN filters, Equation (2.3), are not shown since these matrices are always constant and diagonal.

The rotated process noise covariance for the CV TOPN filter is shown in Figure 5-19. This filter uses the rotation matrix D_k, given in Equation (4.4), which is a function of velocity estimates. The Qr(3,3) remains at a larger value throughout the trajectory than either Qr(1,1) or Qr(2,2). The reason for this is that the rotation of Q_k^{tg} in Equation (4.1) distributes part of the Qr(1,1) and Qr(2,2) to the covariance between X and Y, Qr(1,2). Thus, Qr(1,1) and Qr(2,2) are reduced, and Qr(1,2) is increased. Since the target's velocity vector remains in the XY plane throughout the trajectory, the rotation matrix does not affect Qr(3,3), Qr(1,3), or Qr(2,3).

The rotated process noise covariances of the CA TOPN filter are shown in Figures 5-20 through 5-22. This filter uses the rotation matrix D_k, given in Equation (4.2), which is a function of velocity estimates and acceleration estimates. In Figure 5-20, the target maneuvers in the XY plane, so the lateral acceleration vector remains in the XY plane. Thus, $Qr(1,1)$ and $Qr(2,2)$ remain at their maximum value. The $Qr(3,3)$ remains at a small value since this is the direction orthogonal to the plane of motion, and the variance in this direction, q_k^{ll}, was set to a small value (see Table 5-3 and Equation (4.1)). In Figure 5-21, the target maneuvers in a plane slanted 45 degrees with respect to the XY plane. The $Qr(1,1)$ remains at its maximum value. The $Qr(2,2)$ and $Qr(3,3)$ were reduced by half, and the covariance between them, $Qr(2,3)$, was increased. In Figure 5-22, the target performs a maneuver similar to the one in Figure 20, but at a longer range. Thus, all the process noise variances behave in a manner similar to Figure 20. The strange behavior of $Qr(1,3)$ and $Qr(2,3)$ in Figures 5-20 and 5-22 is not understood at this time, but the magnitude of these anomalies is so small that no explanation is warranted.

The rotated process noise covariances of the MJ TOPN filter are shown in Figures 5-23 through 5-25. These covariances behave in a similar manner to the CA TOPN filter. This is to be expected since both filters used the same trajectories and the same rotation matrices.

Position Error Ellipses

The position error ellipses calculated for a single time step from a single run of the TOPN and SPN filters are shown in Figures 5-26 through 5-32. These position error ellipses are typical of ones which would be used to validate measurements in a cluttered environment. These error ellipses were calculated from the filtered error covariances at the 100^{th} time step during a single run of each filter, as discussed in Appendix B. The 100^{th} time step was arbitrarily chosen to compare the relative sizes between position error ellipses calculated from SPN and TOPN filter covariances. Both the horizontal and vertical position ellipses are shown, so that the volume of the position error ellipsoids can be estimated. As demonstrated in Figure 5-26, the CV TOPN filter has a slightly smaller ellipse than the CV SPN filter in the XY plane. As shown in Figures 5-27 through 5-29, the CA TOPN filter reduces the size of some of the ellipses. In Figures 5-27 and 5-29, only the XZ plane ellipse is smaller since the target's maneuver is confined to the XY plane. In Figure 5-28, both the XY and XZ

plane ellipses are smaller since the target's maneuver is confined to a plane at a 45 degree angle to the Y and Z axes. The MJ TOPN filter's position error ellipses shown in Figures 5-30 through 5-32 were similar to those of the CA TOPN filter.

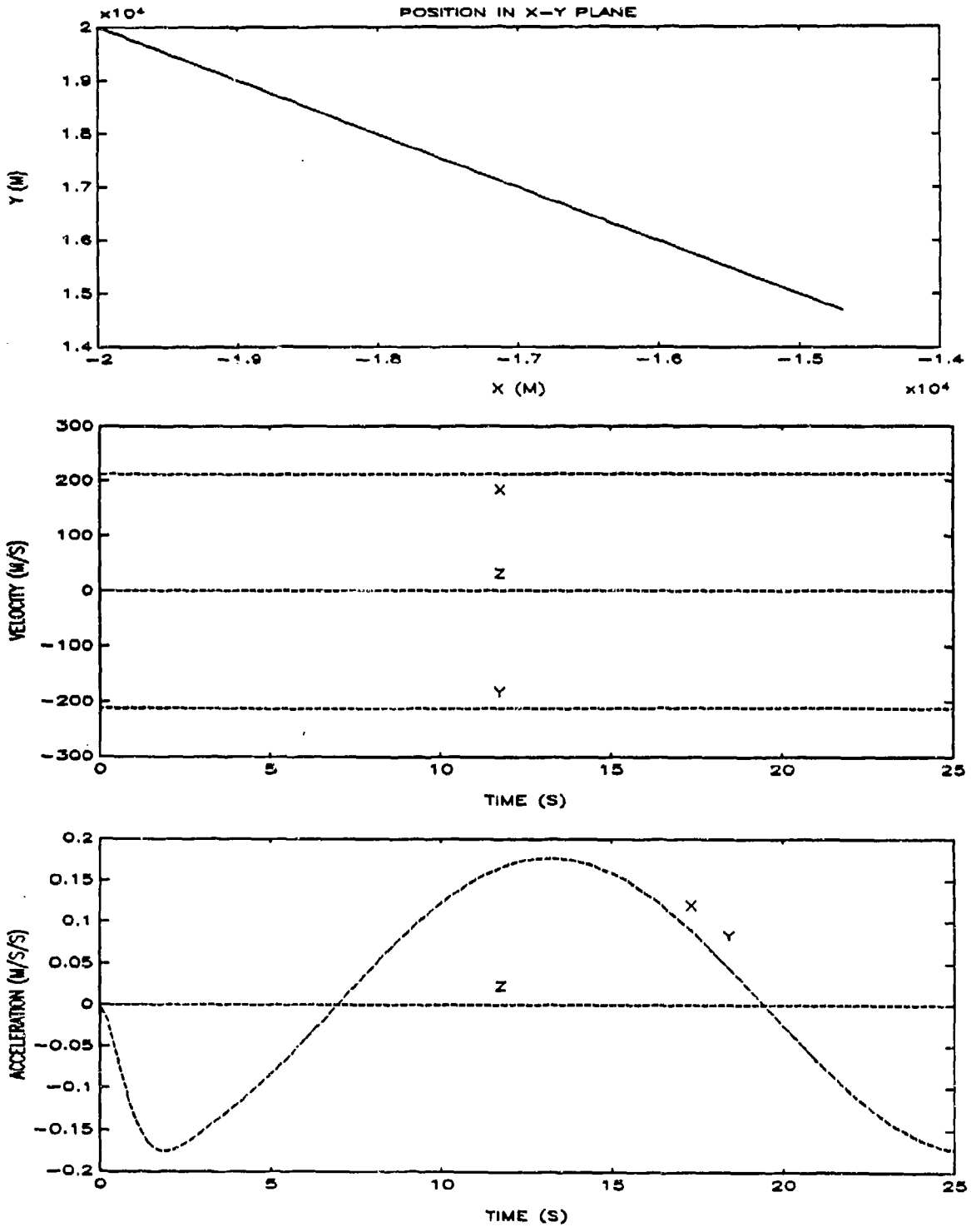

FIGURE 5-1. TRAJECTORY 1

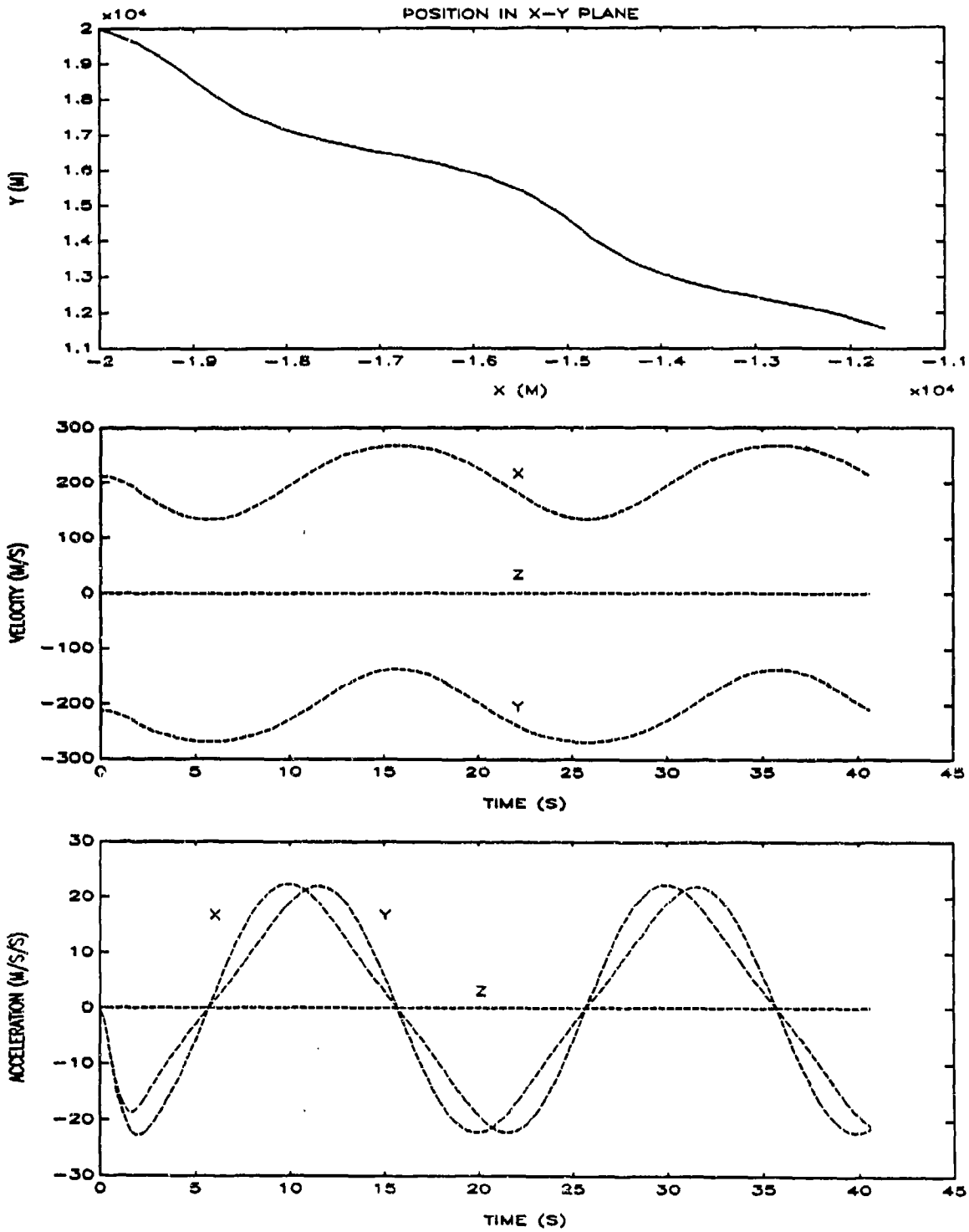

FIGURE 5-2. TRAJECTORY 2

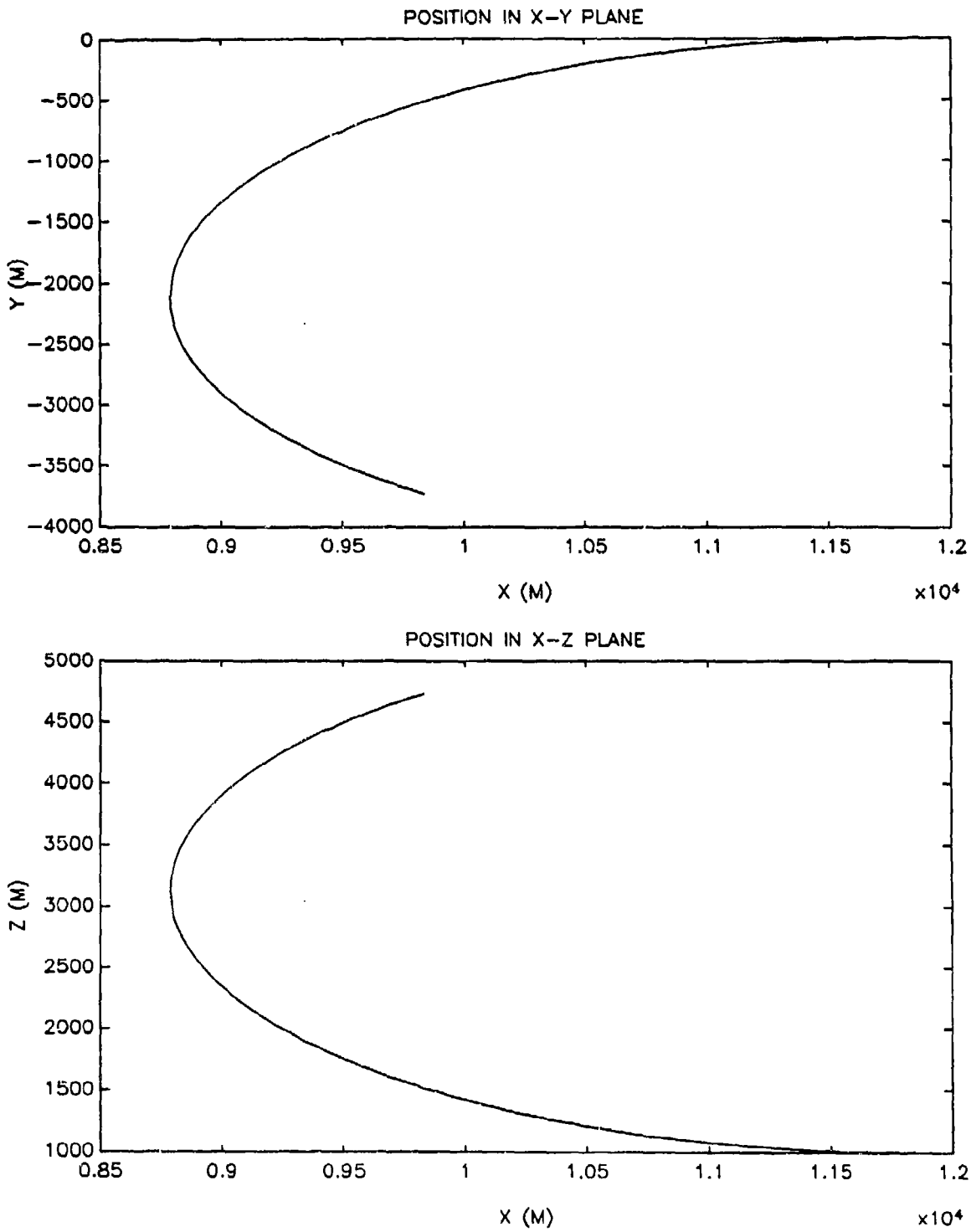

FIGURE 5-3. TRAJECTORY 3

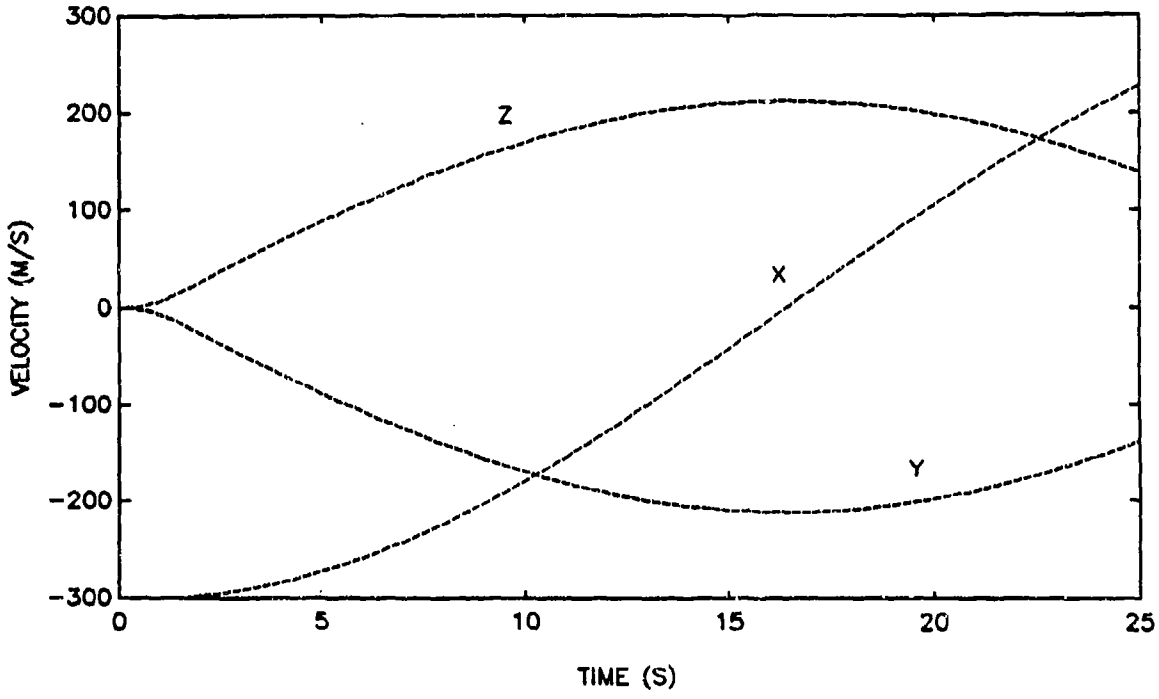

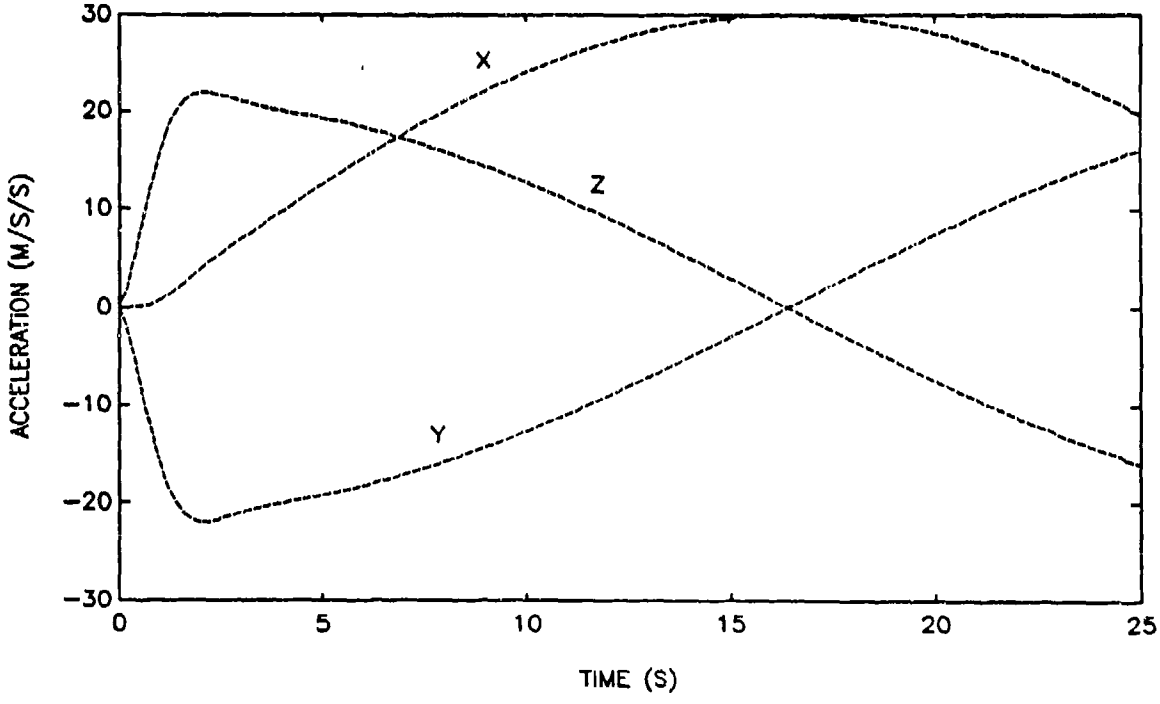

FIGURE 5-3. TRAJECTORY 3 (Continued)

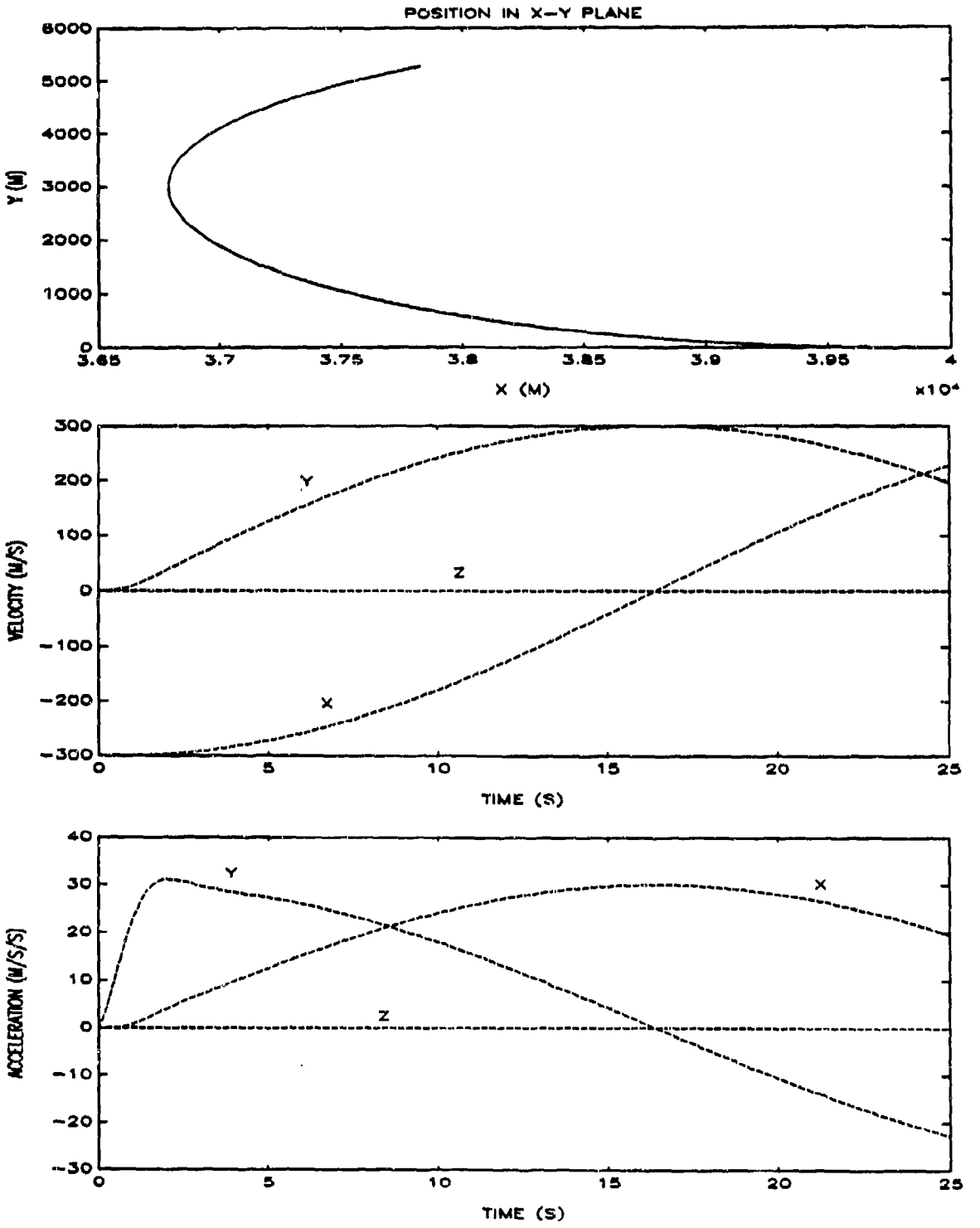

FIGURE 5-4. TRAJECTORY 4

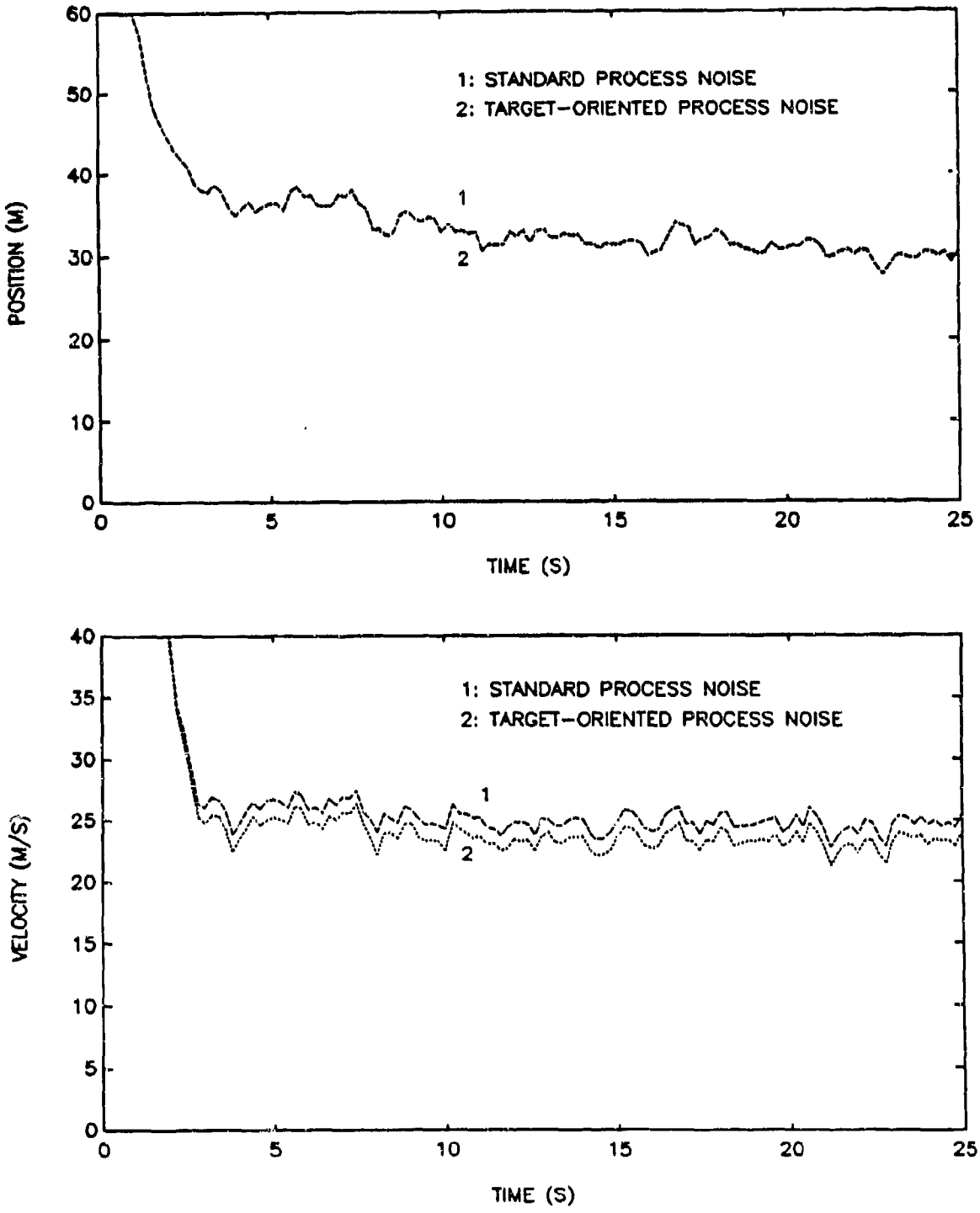

FIGURE 5-5. RMS ERRORS FOR CV FILTER - TRAJ 1

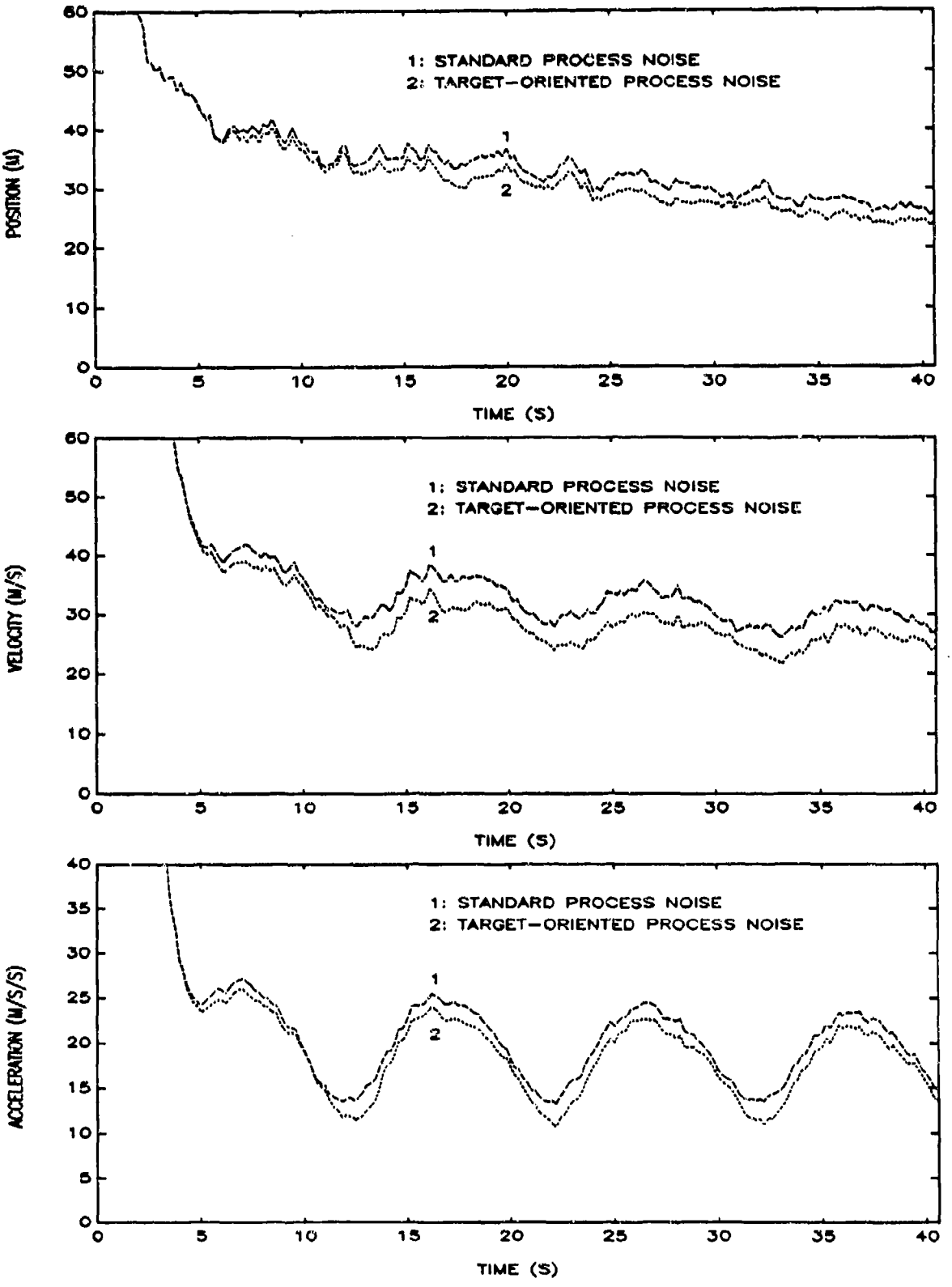

FIGURE 5-6. RMS ERRORS FOR CA FILTER - TRAJ 2

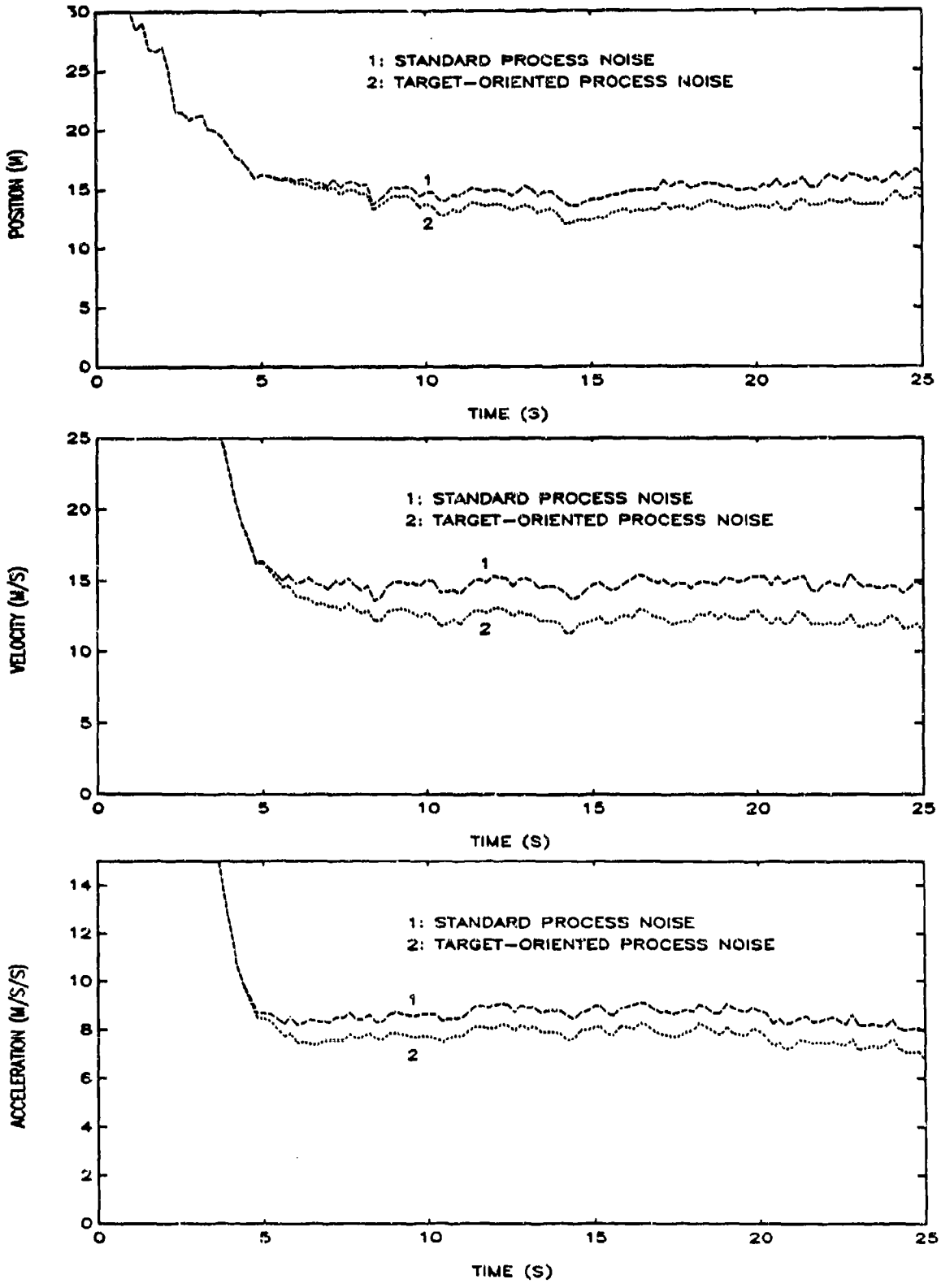

FIGURE 5-7. RMS ERRORS FOR CA FILTER - TRAJ 3

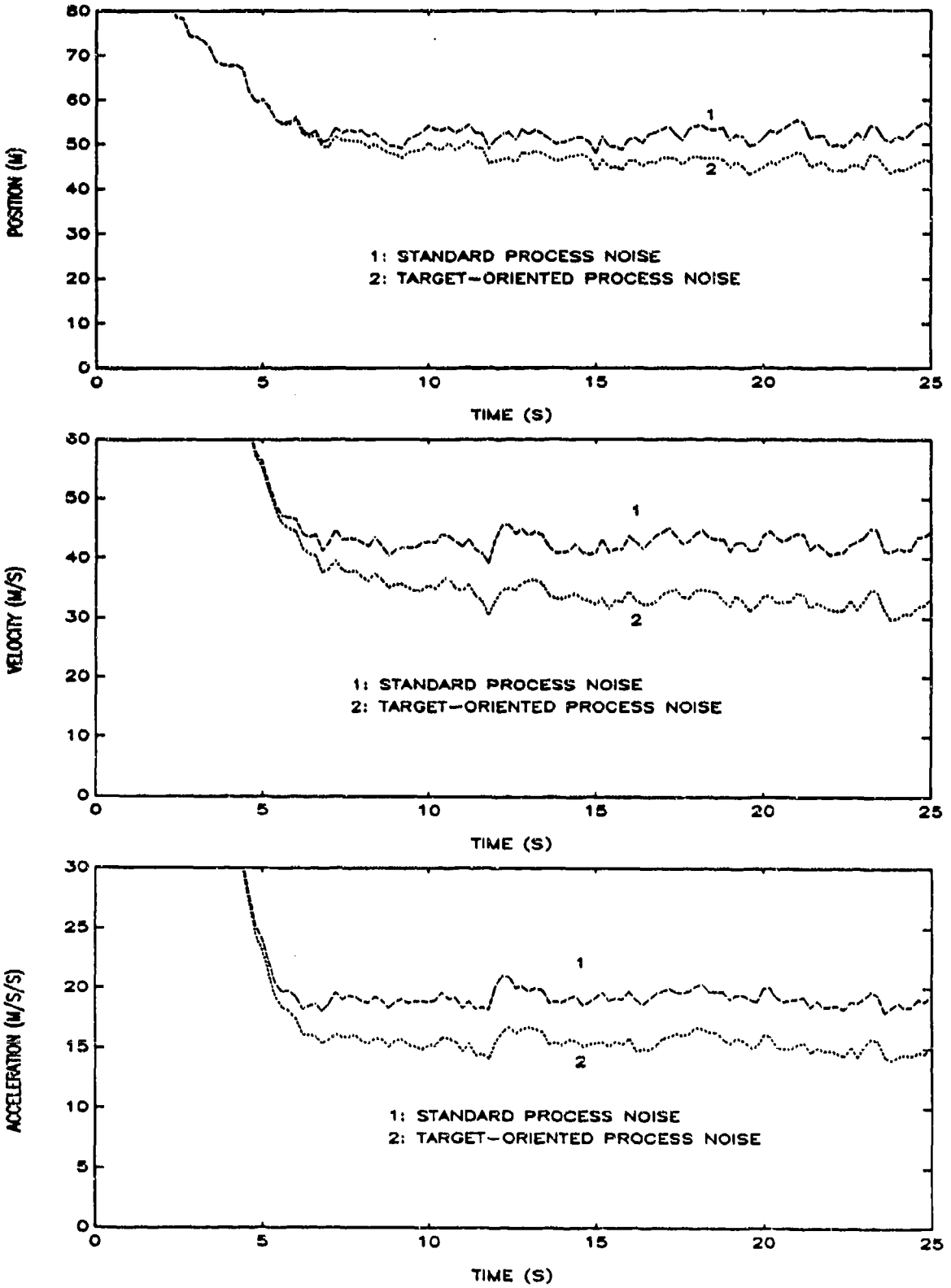

FIGURE 5-8. RMS ERRORS FOR CA FILTER - TRAJ 4

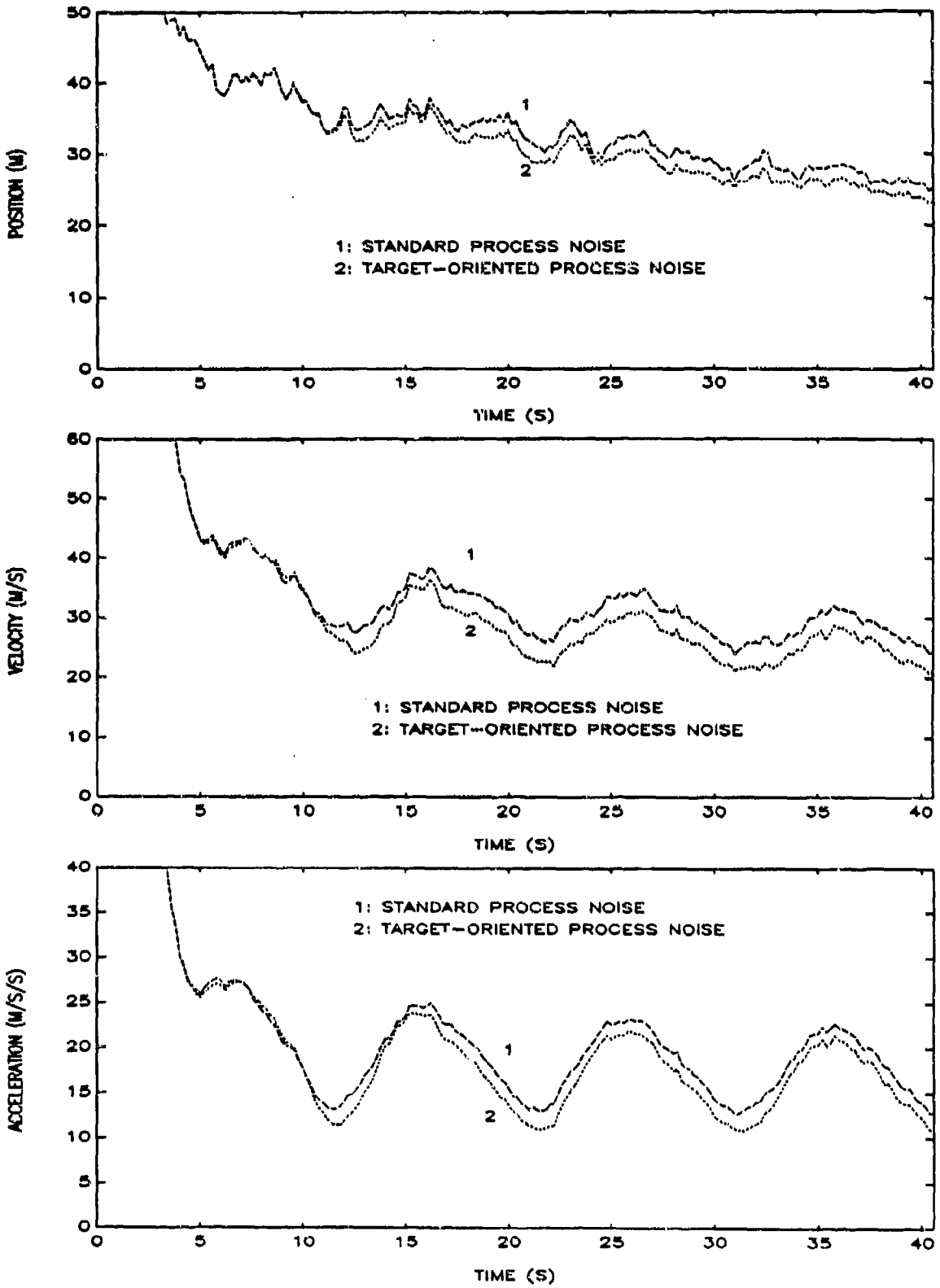

FIGURE 5-9. RMS ERRORS FOR MJ FILTER - TRAJ 2

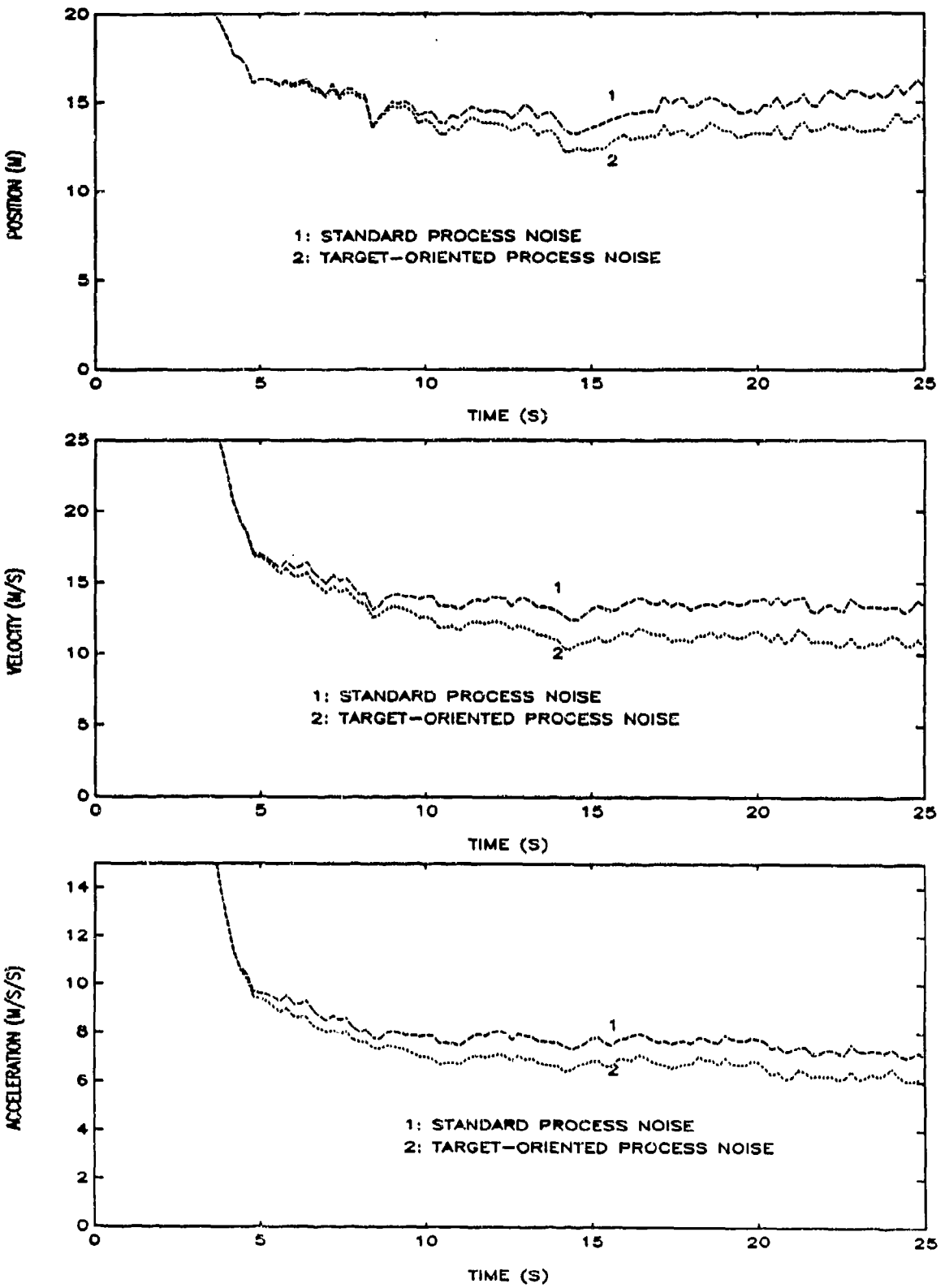

FIGURE 5-10. RMS ERRORS FOR MJ FILTER - TRAJ 3

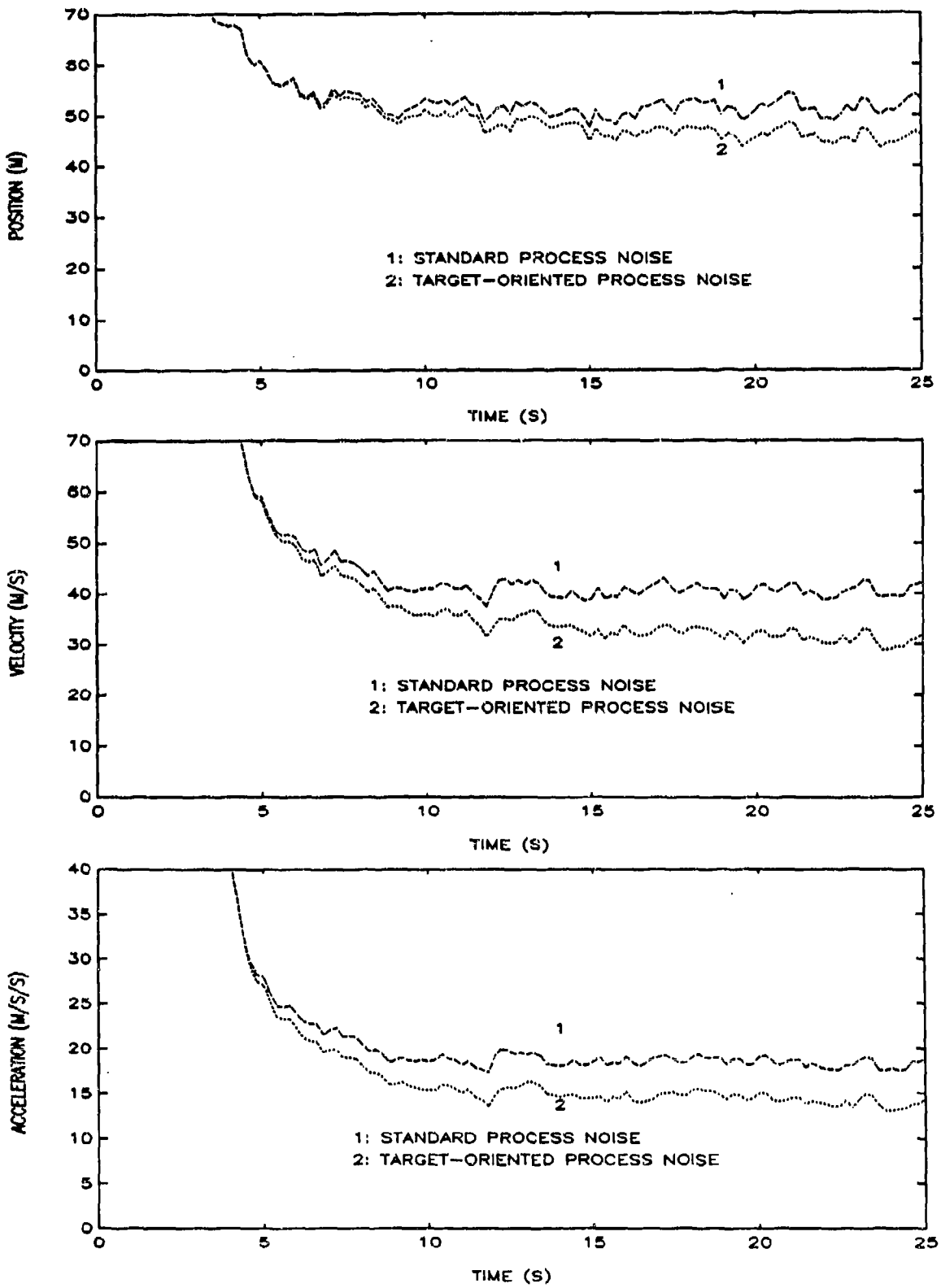

FIGURE 5-11. RMS ERRORS FOR MJ FILTER - TRAJ 4

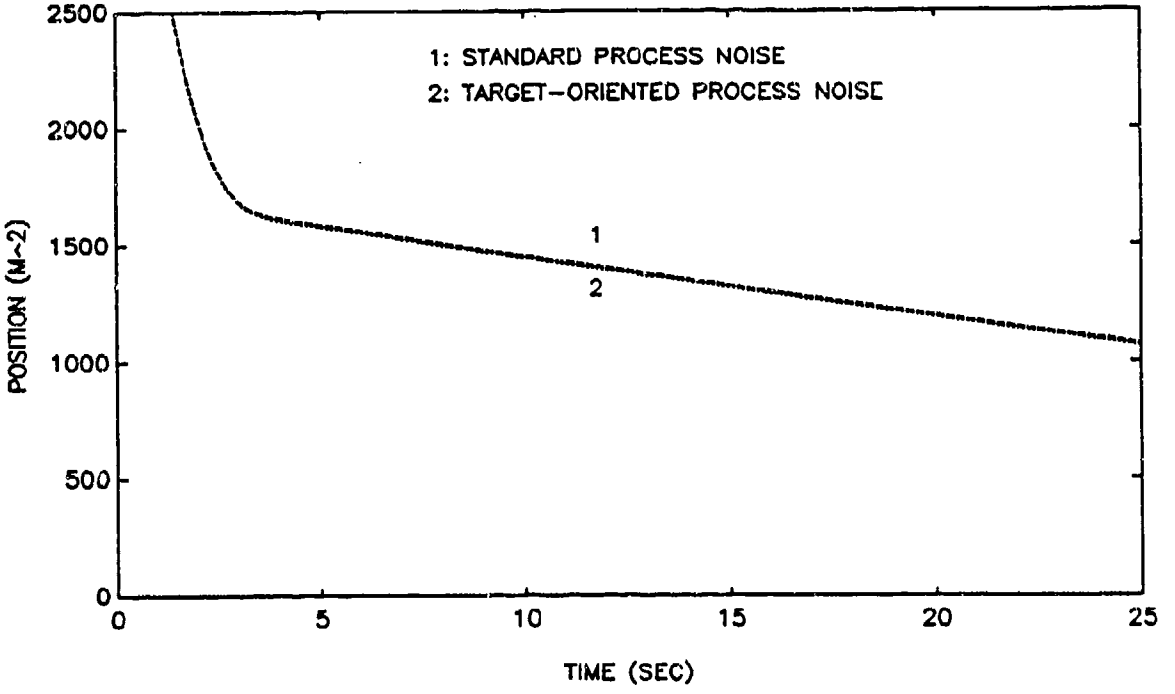

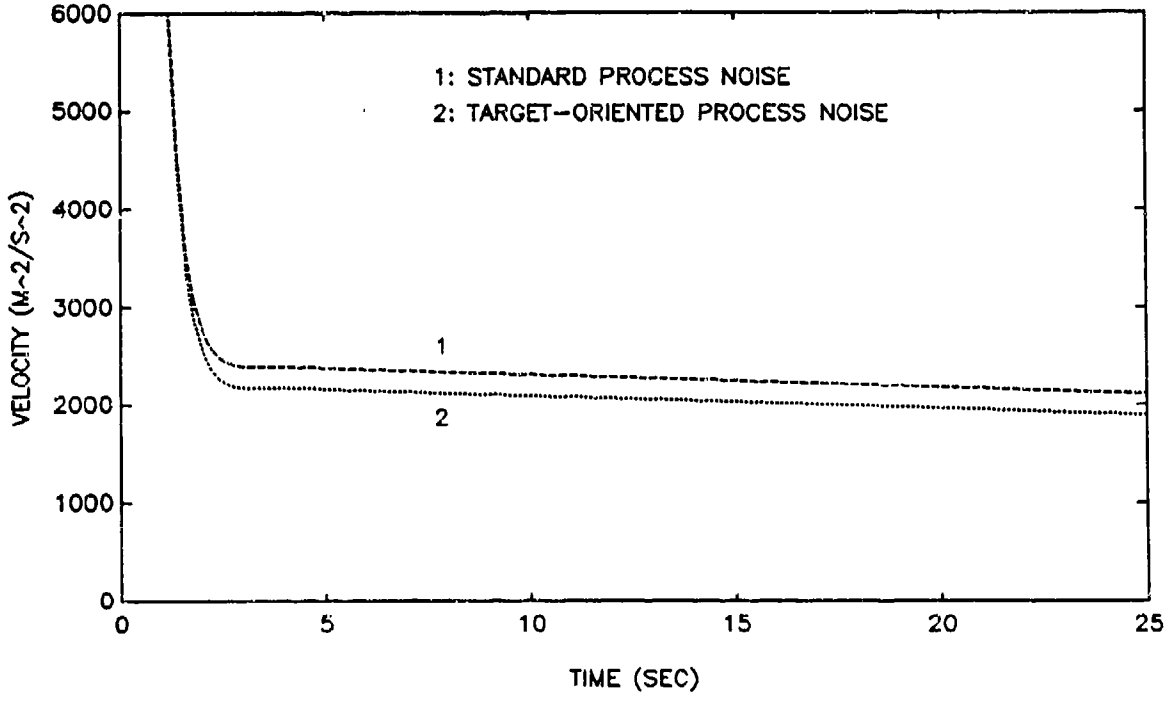

FIGURE 5-12. FILTERED ERROR COVARIANCES FOR CV FILTER - TRAJ 1

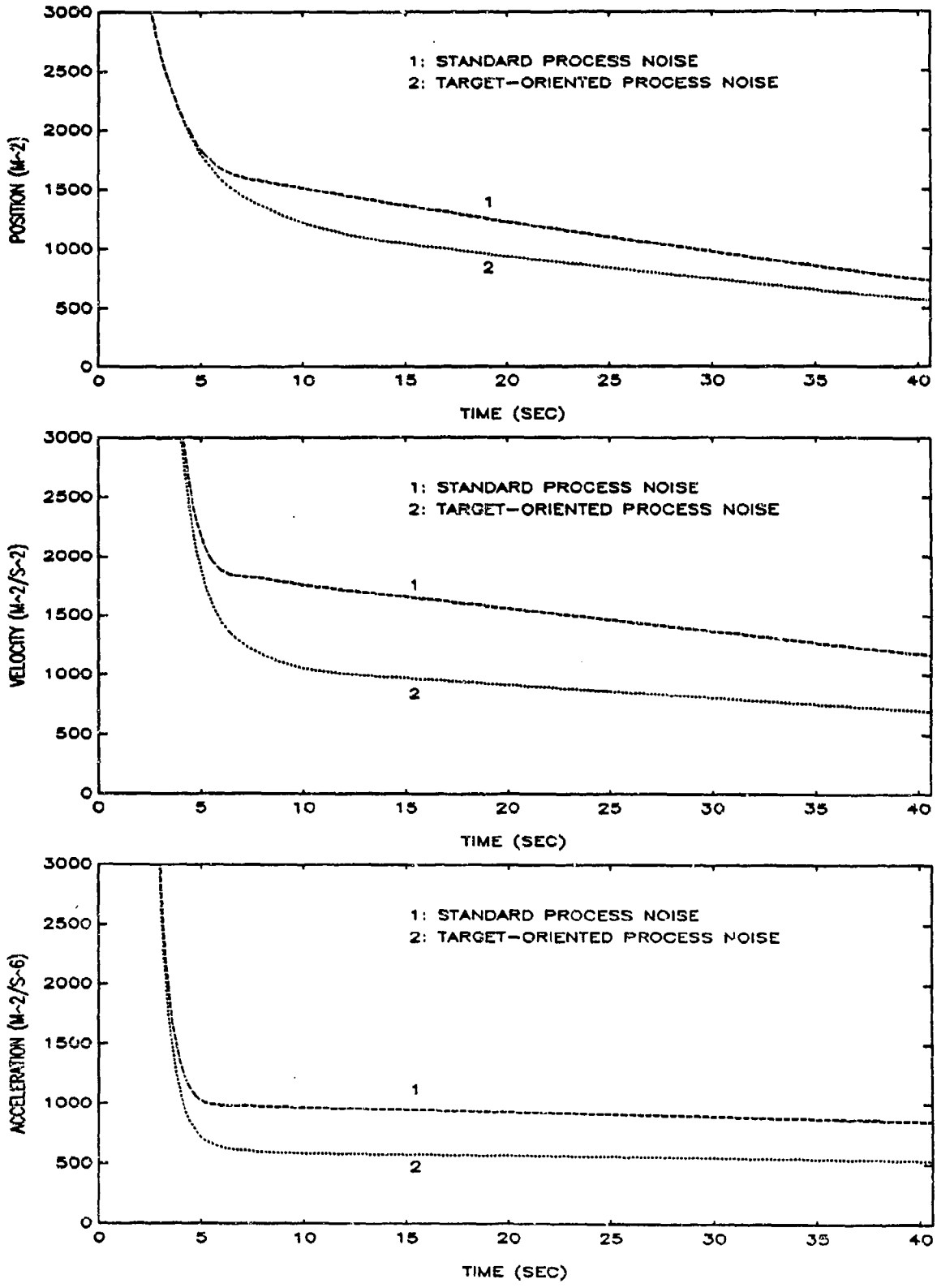

FIGURE 5-13. FILTERED ERROR COVARIANCES FOR CA FILTER - TRAJ 2

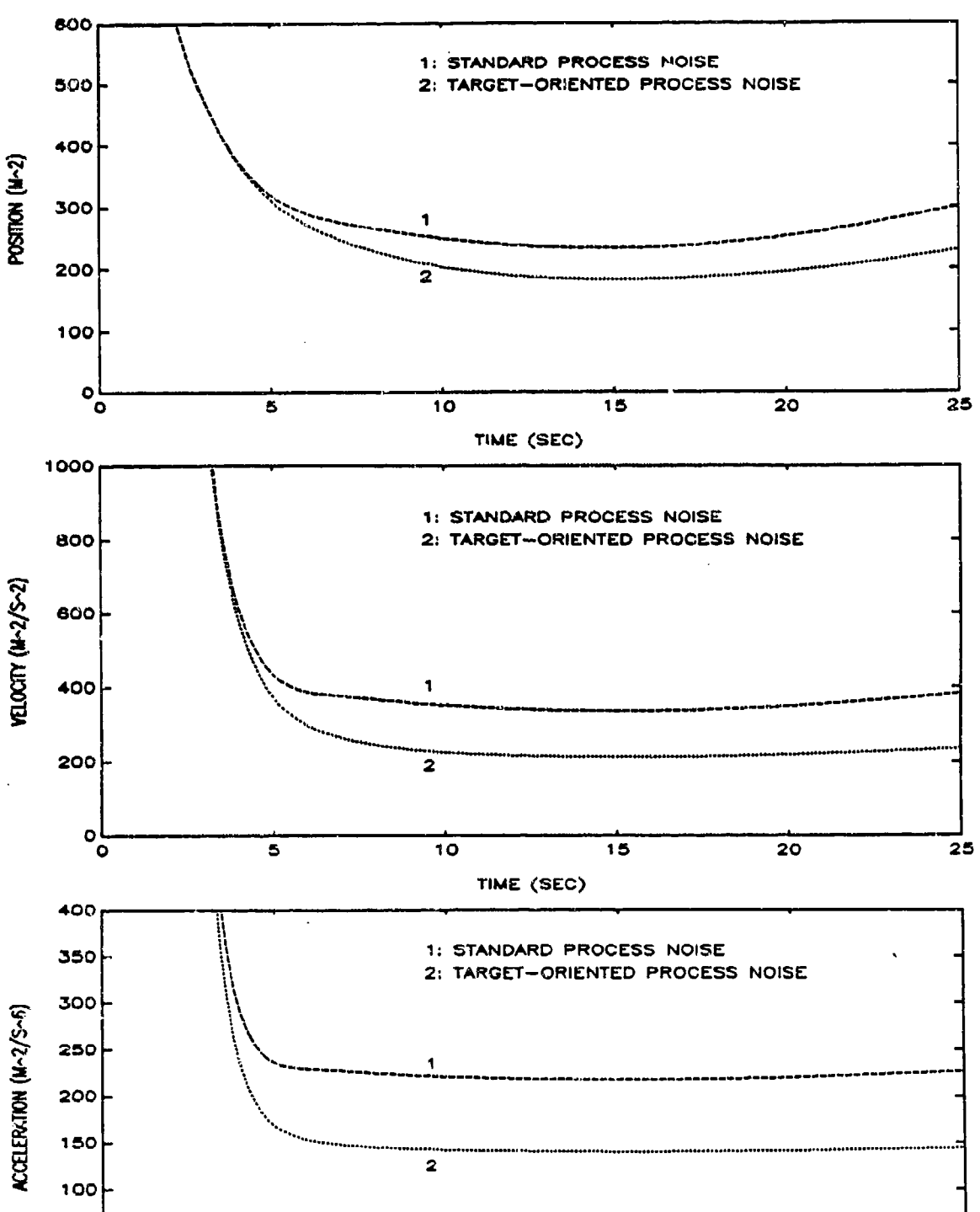

FIGURE 5-14. FILTERED ERROR COVARIANCES FOR CA FILTER - TRAJ 3

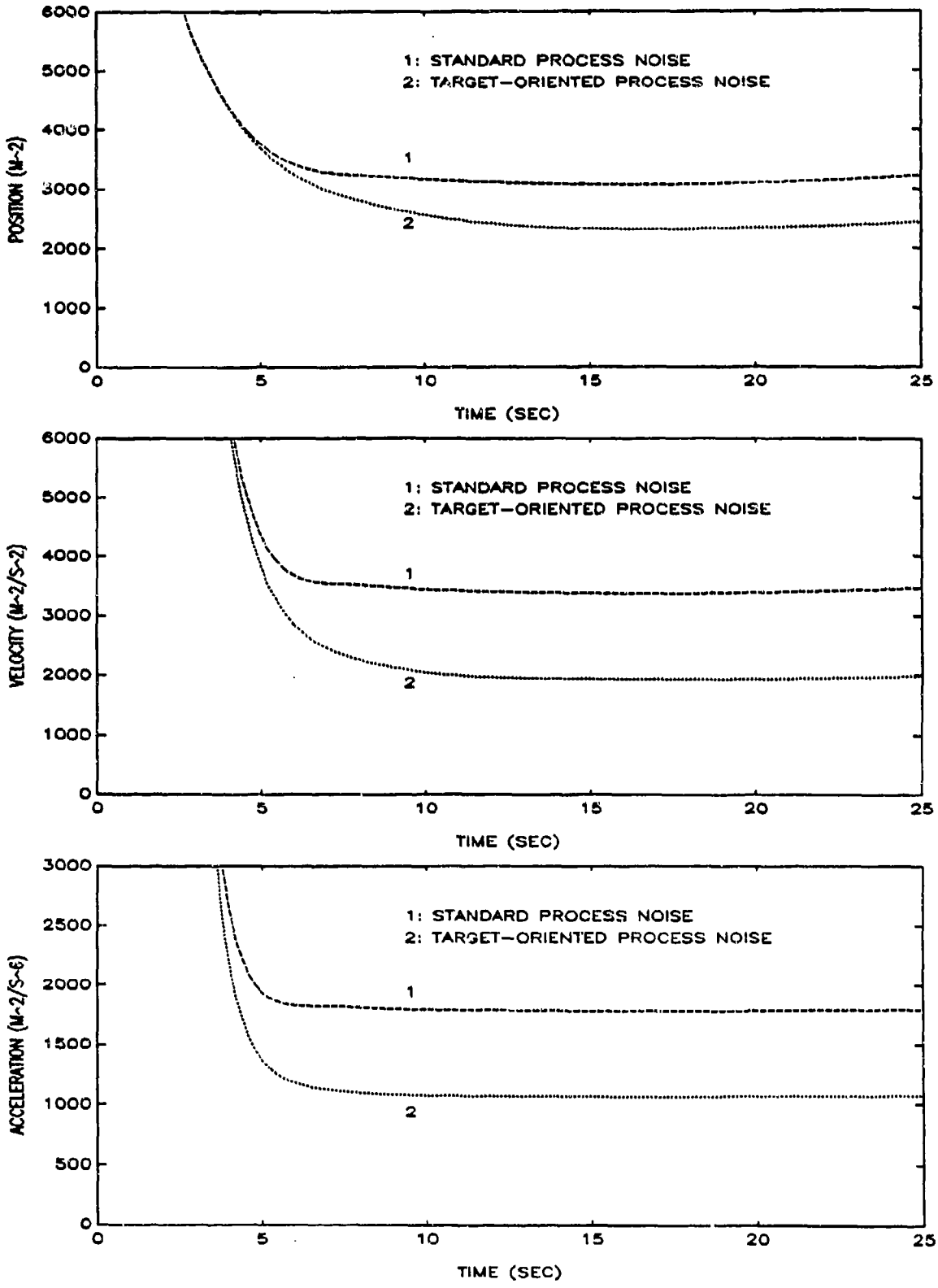

FIGURE 5-15. FILTERED ERROR COVARIANCES FOR CA FILTER - TRAJ 4

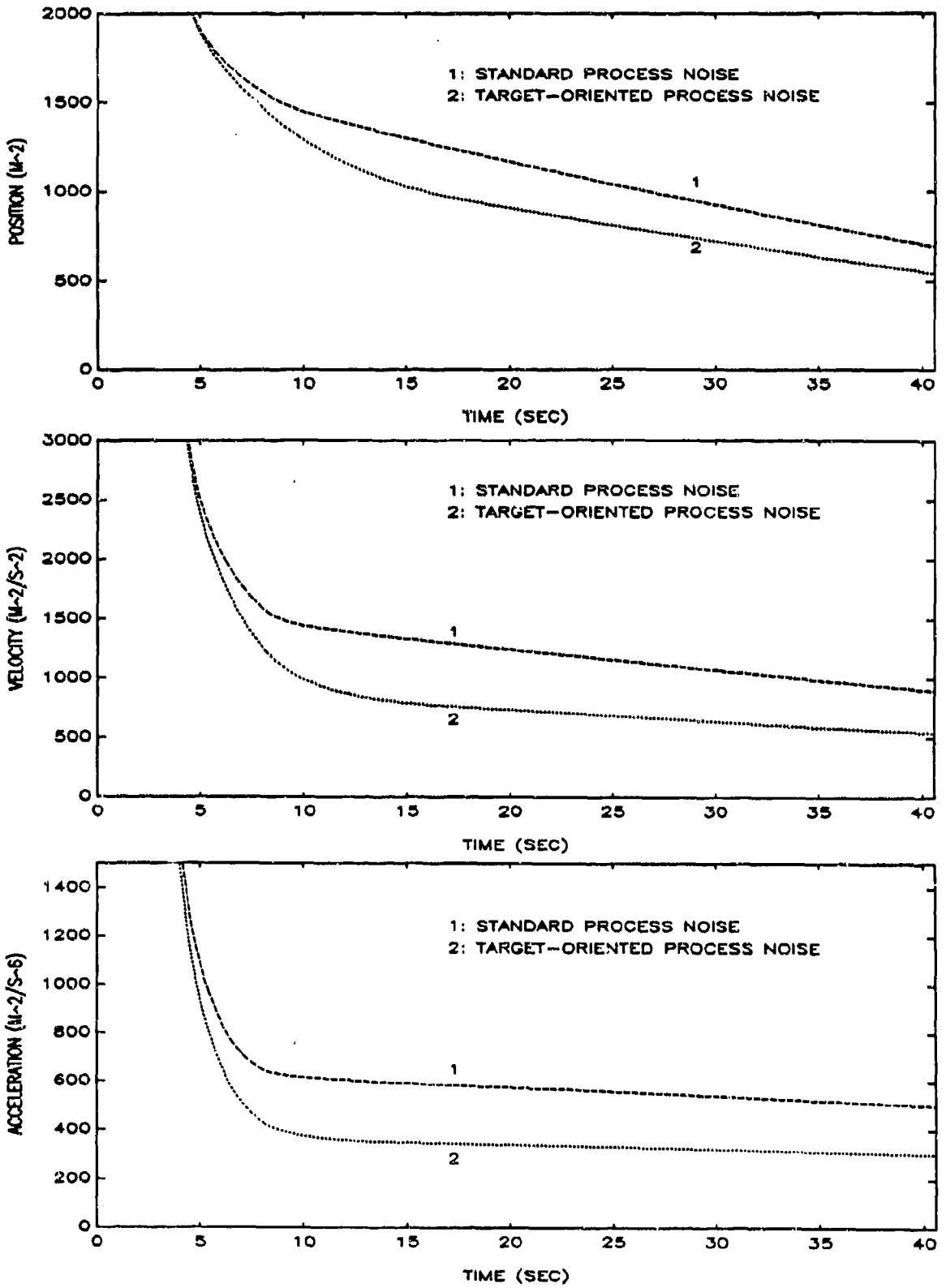

FIGURE 5-16. FILTERED ERROR COVARIANCES FOR MJ FILTER - TRAJ 2

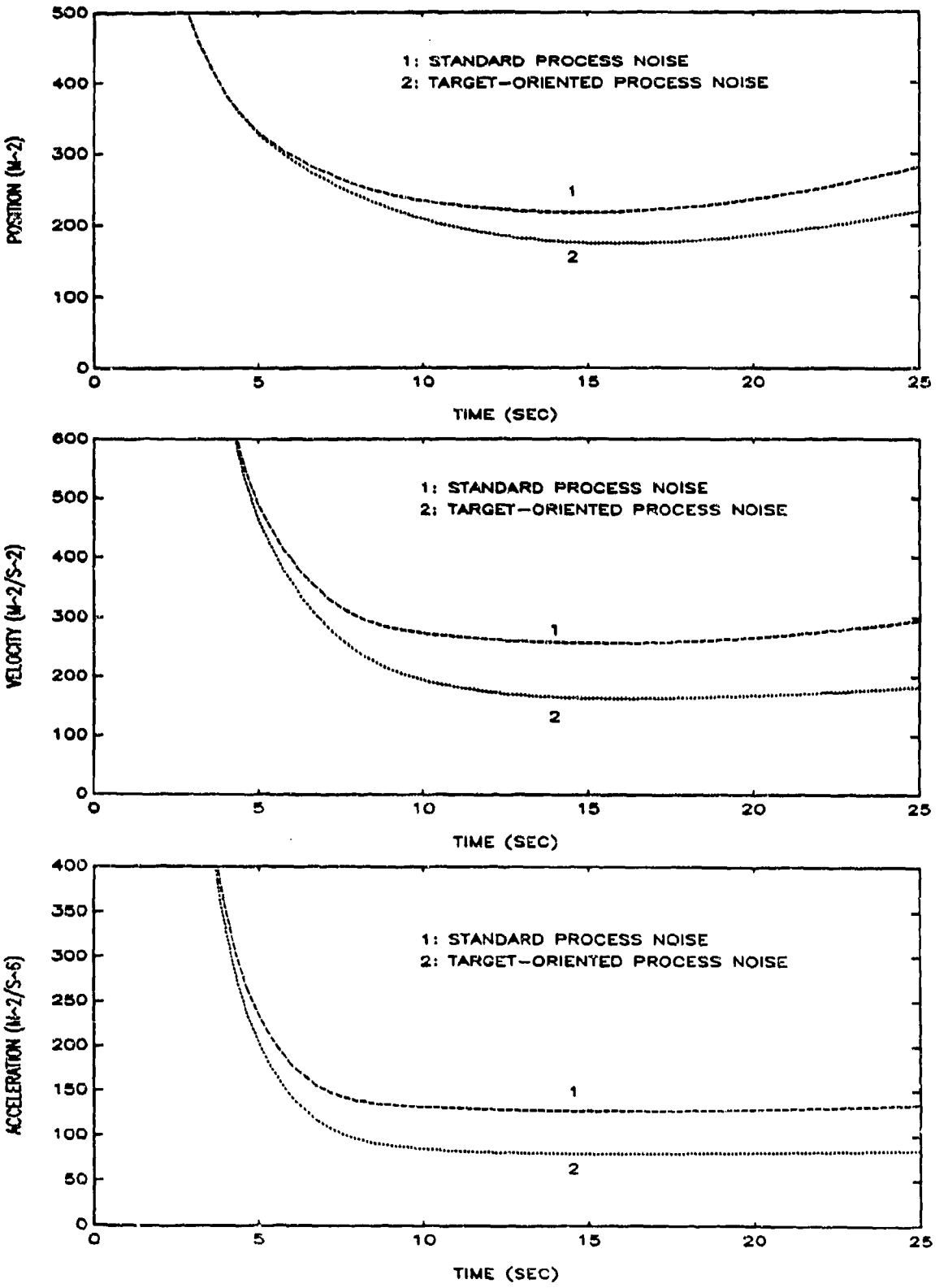

FIGURE 5-17. FILTERED ERROR COVARIANCES FOR MJ FILTER - TRAJ 3

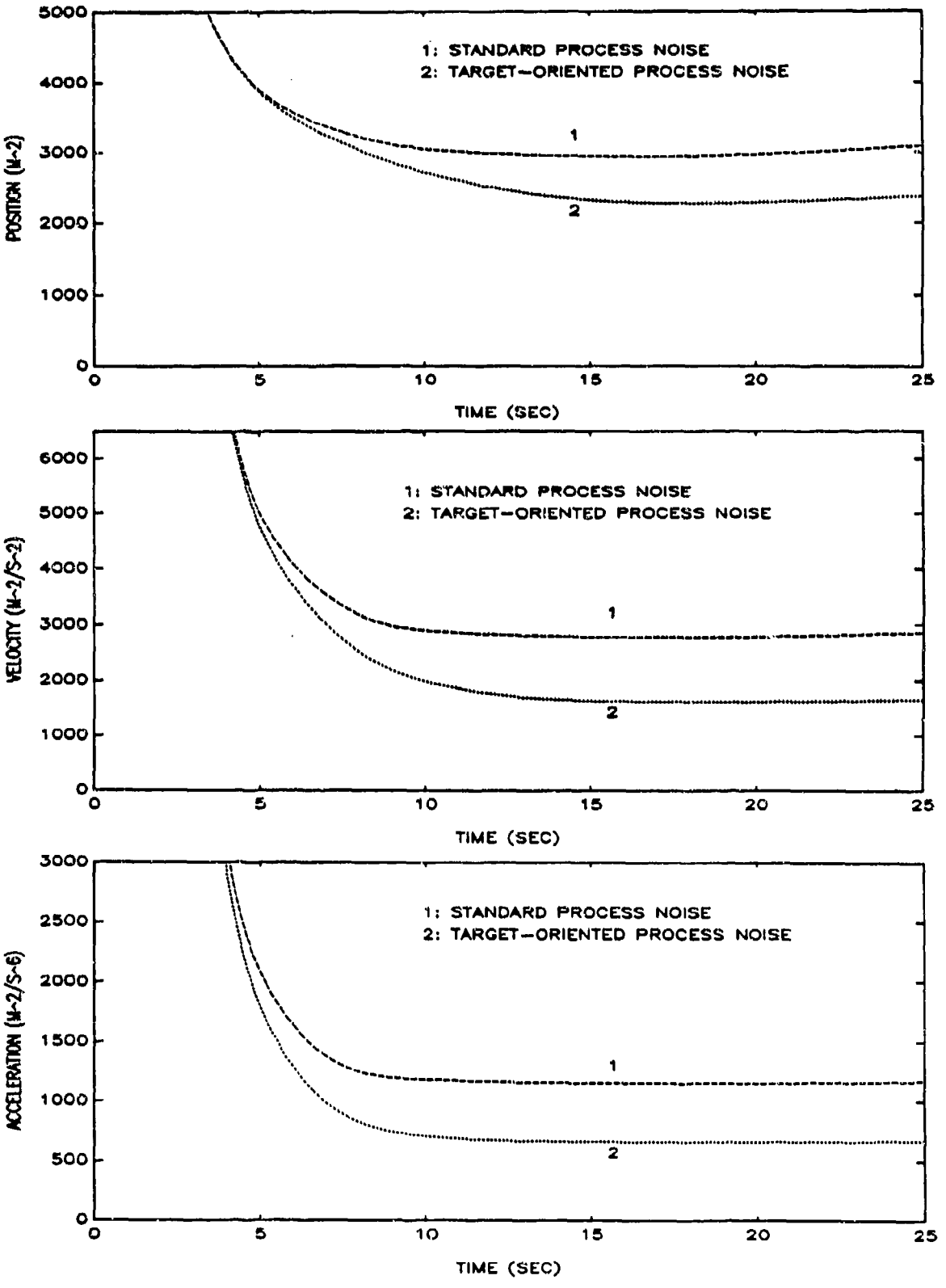

FIGURE 5-18. FILTERED ERROR COVARIANCES FOR MJ FILTER - TRAJ 4

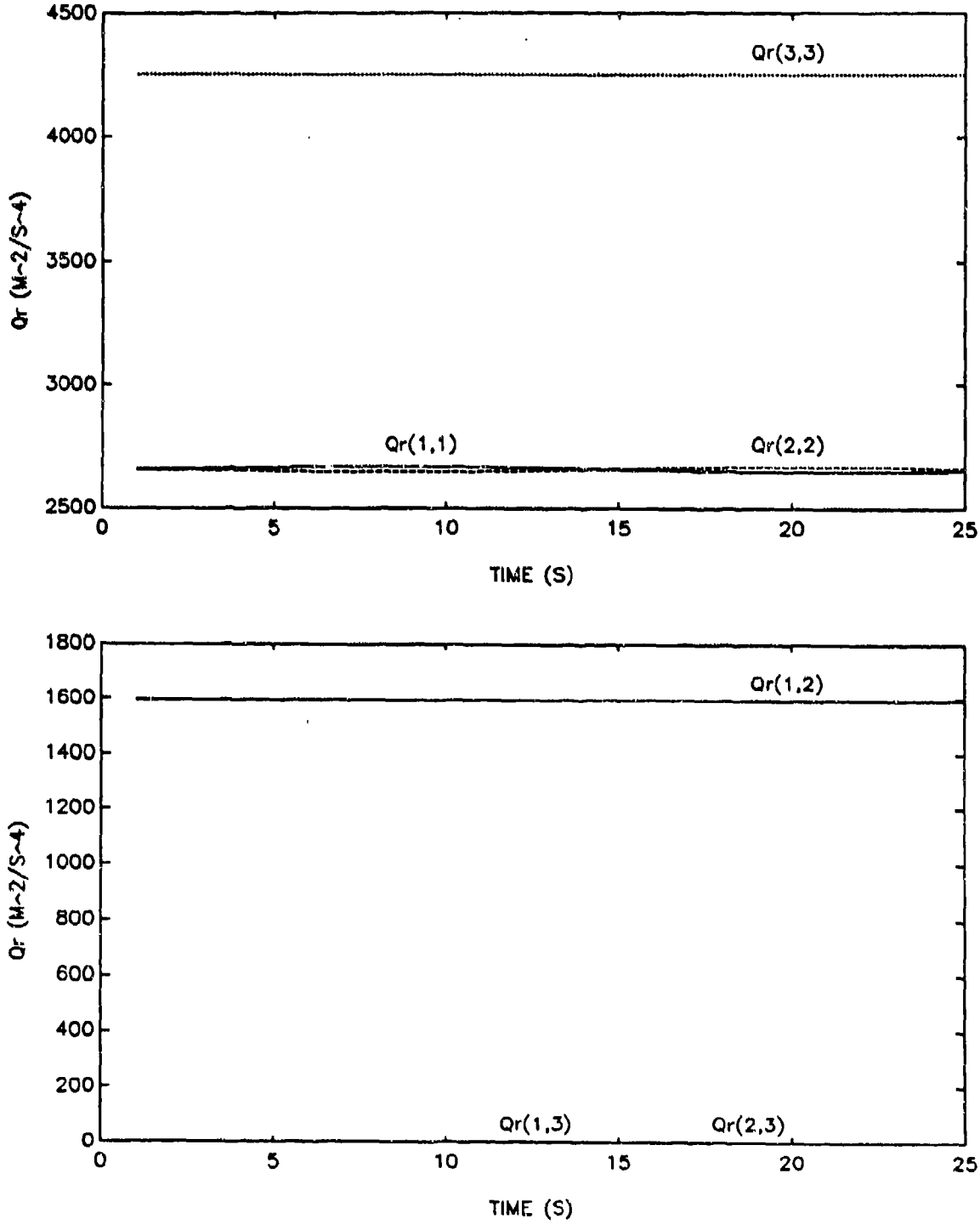

FIGURE 5-19. ROTATED PROCESS NOISE COVARIANCES FOR CV FILTER - TRAJ 1

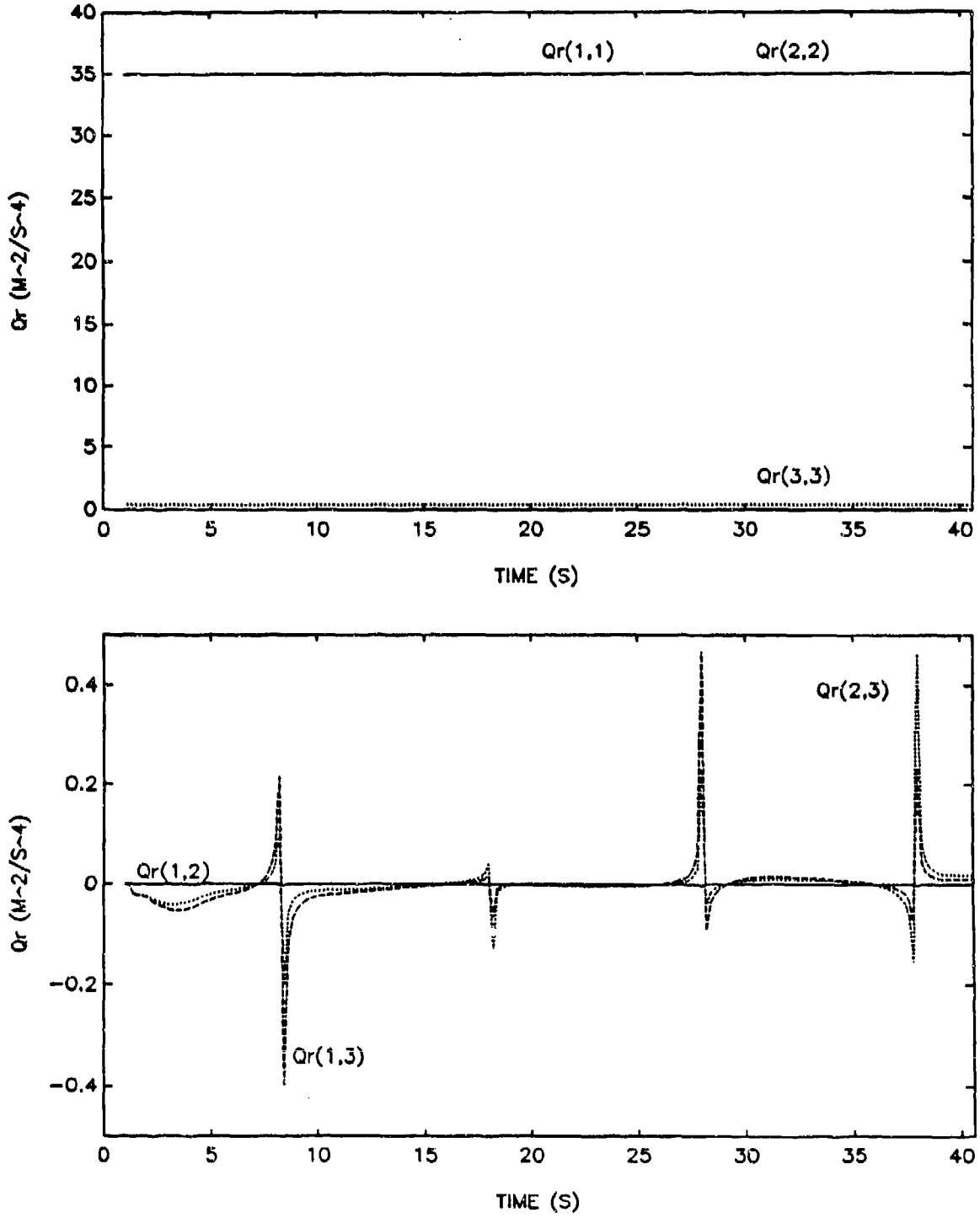

FIGURE 5-20. ROTATED PROCESS NOISE COVARIANCES FOR CA FILTER - TRAJ 2

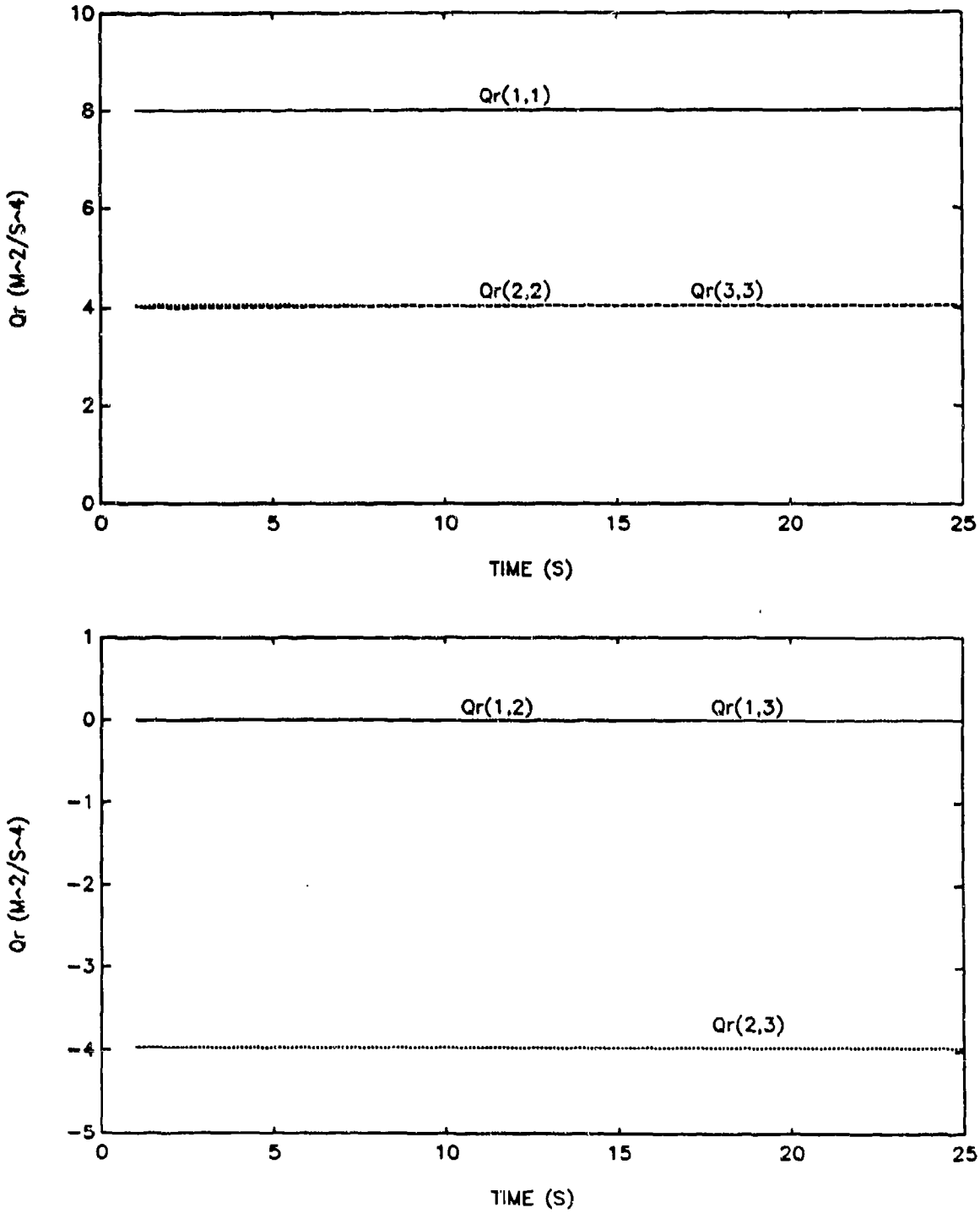

FIGURE 5-21. ROTATED PROCESS NOISE COVARIANCES FOR CA FILTER - TRAJ 3

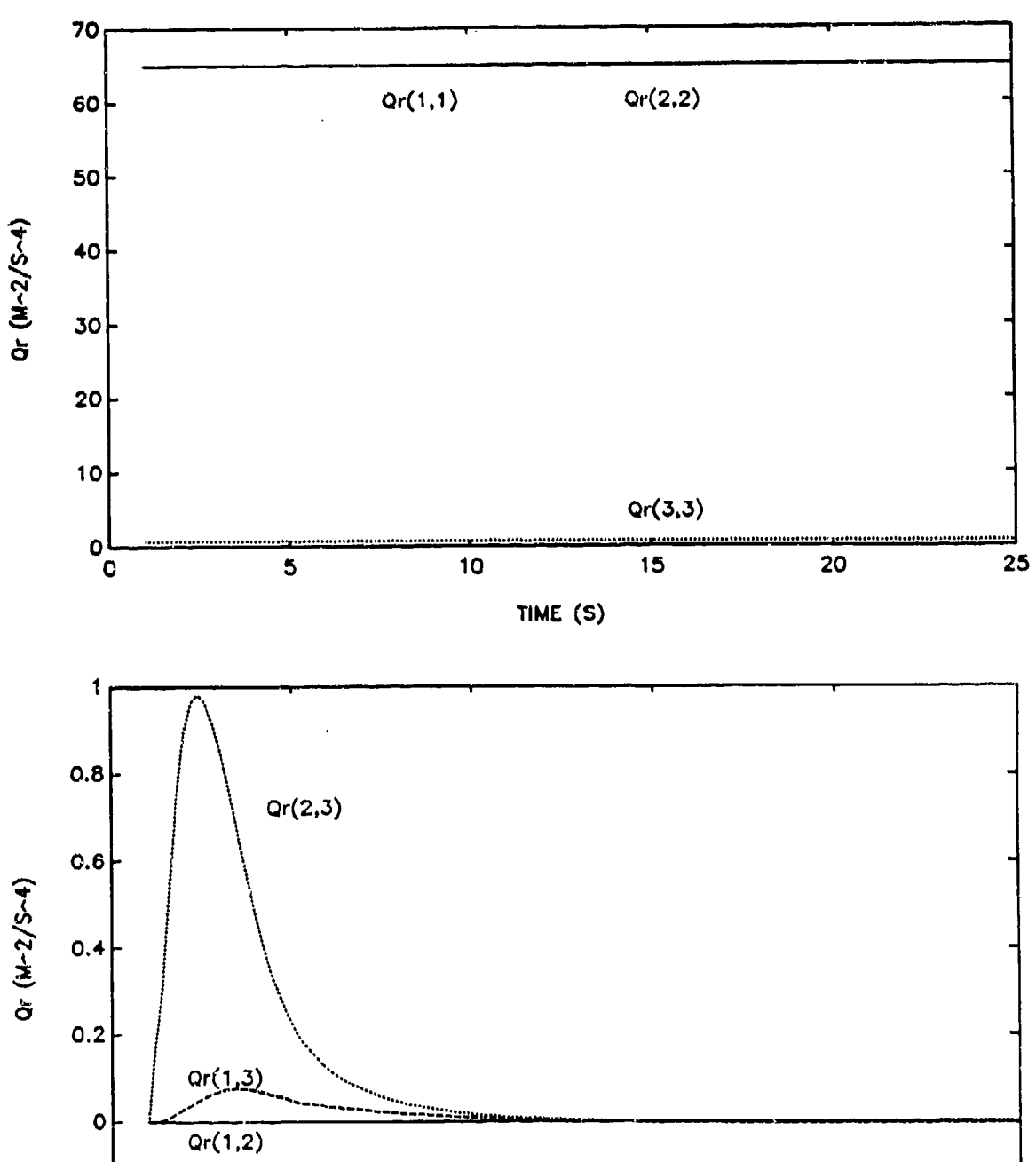

FIGURE 5-22. ROTATED PROCESS NOISE COVARIANCES FOR CA FILTER - TRAJ 4

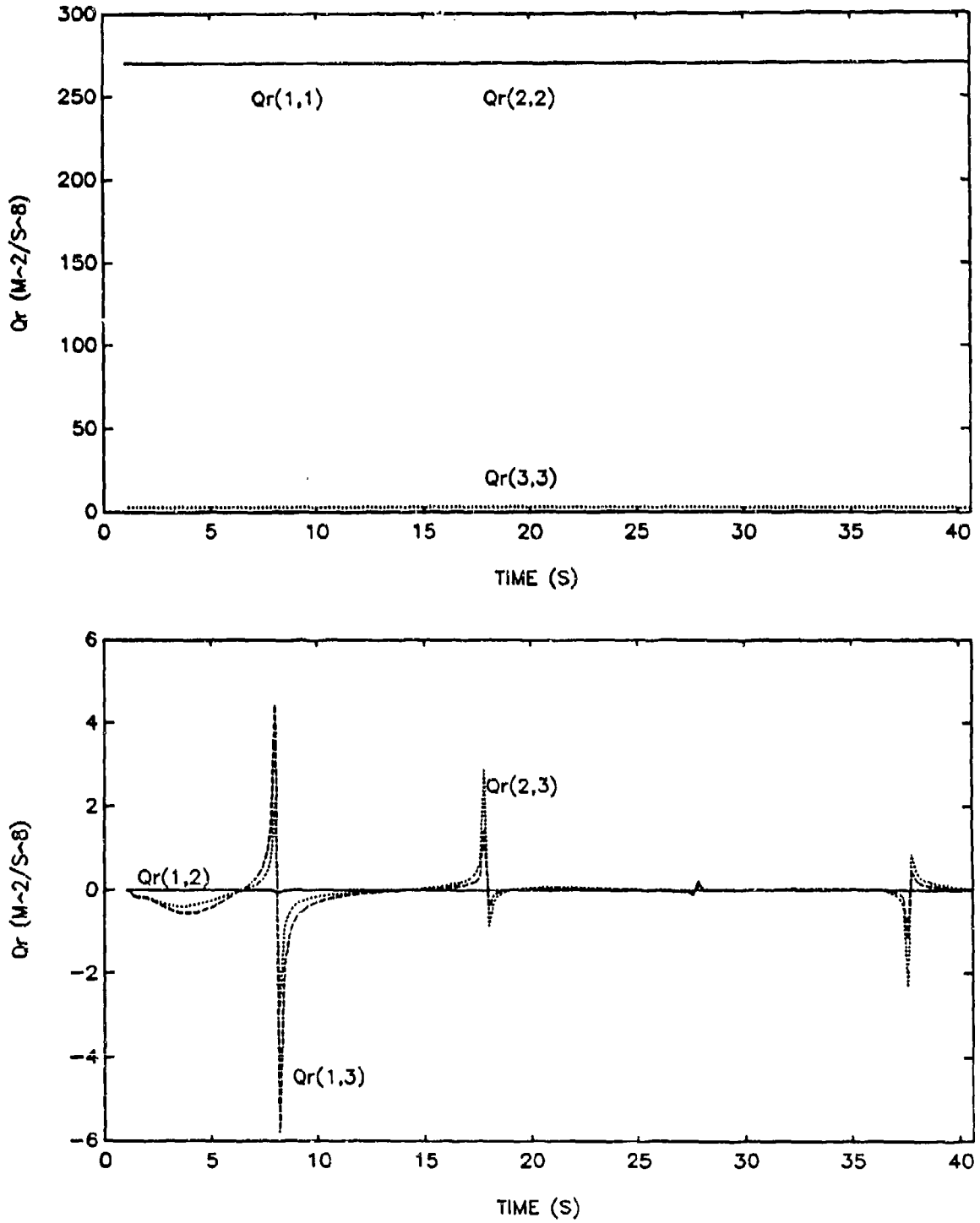

FIGURE 5-23. ROTATED PROCESS NOISE COVARIANCES FOR MJ FILTER - TRAJ 2

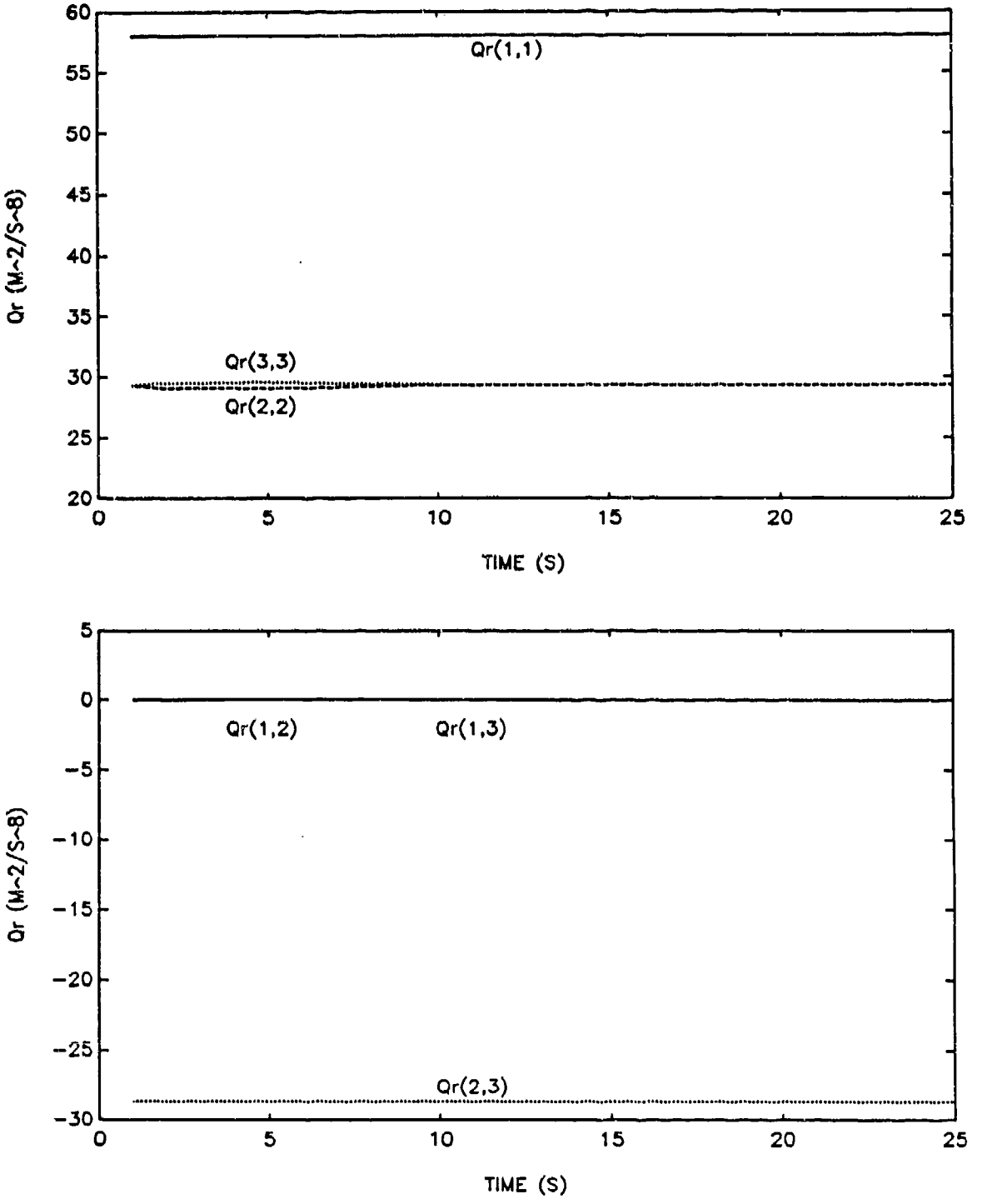

FIGURE 5-24. ROTATED PROCESS NOISE COVARIANCES FOR MJ FILTER - TRAJ 3

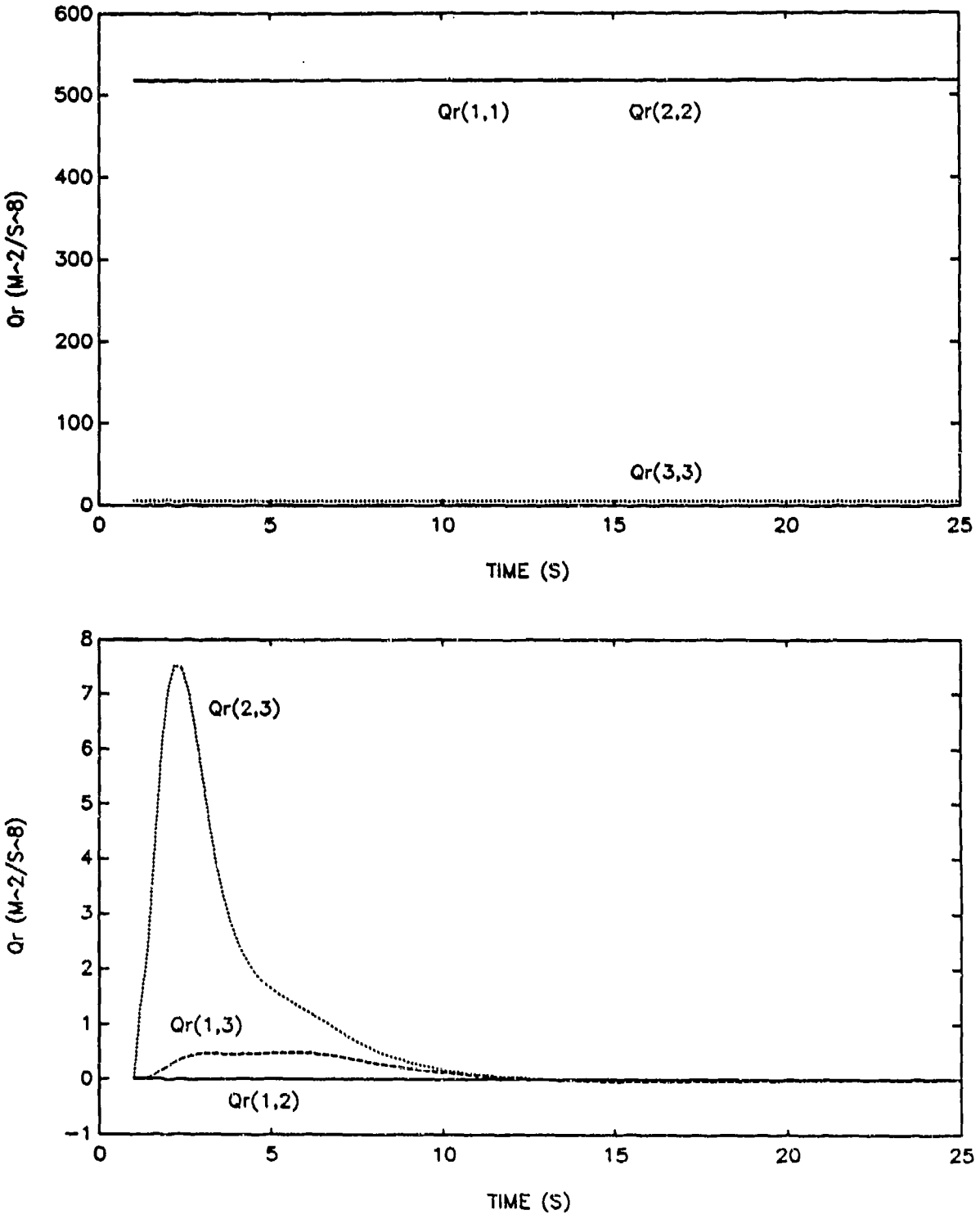

FIGURE 5-25. ROTATED PROCESS NOISE COVARIANCES FOR MJ FILTER - TRAJ 4

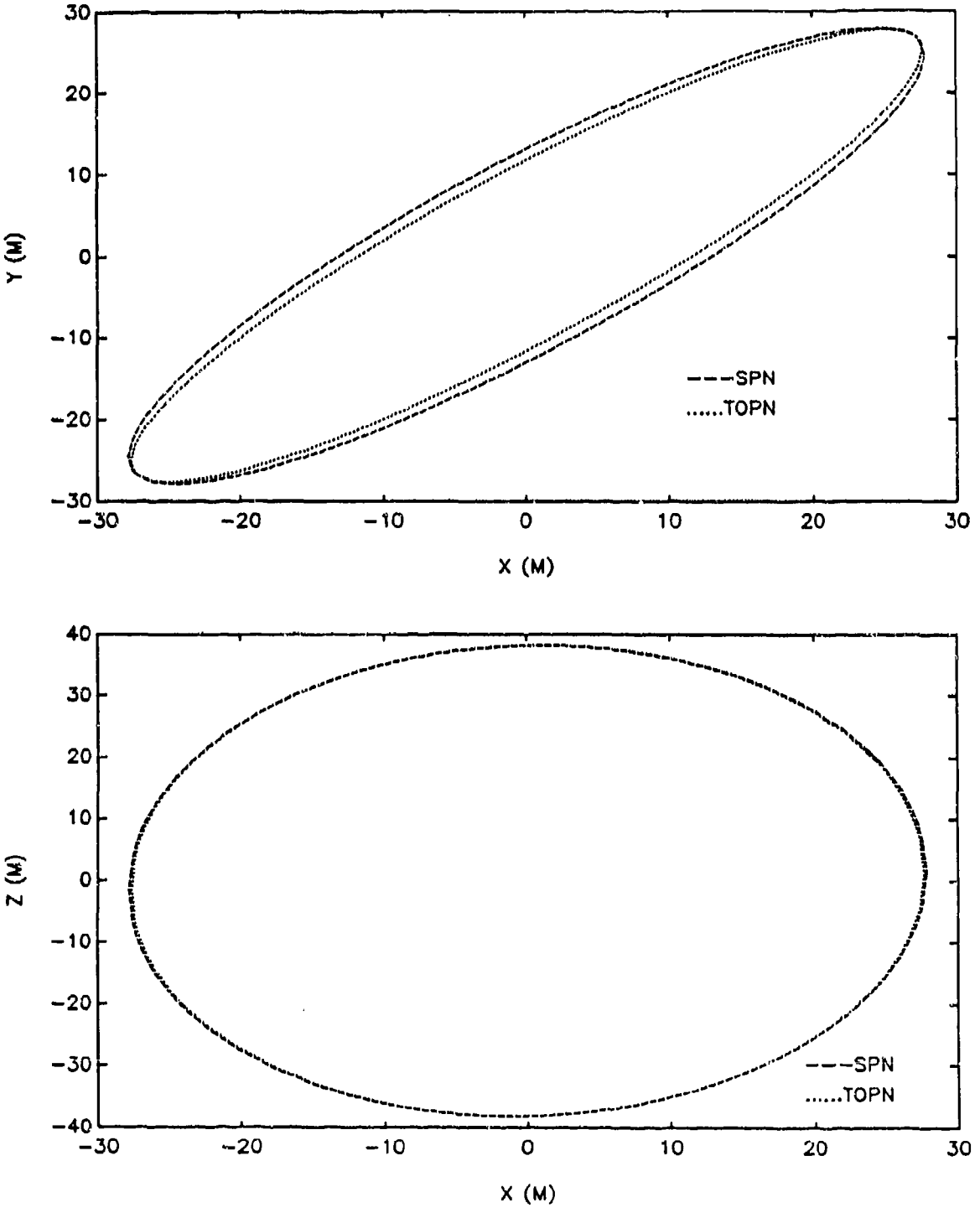

FIGURE 5-26. POSITION ERROR ELLIPSES FOR CV FILTER - TRAJ 1

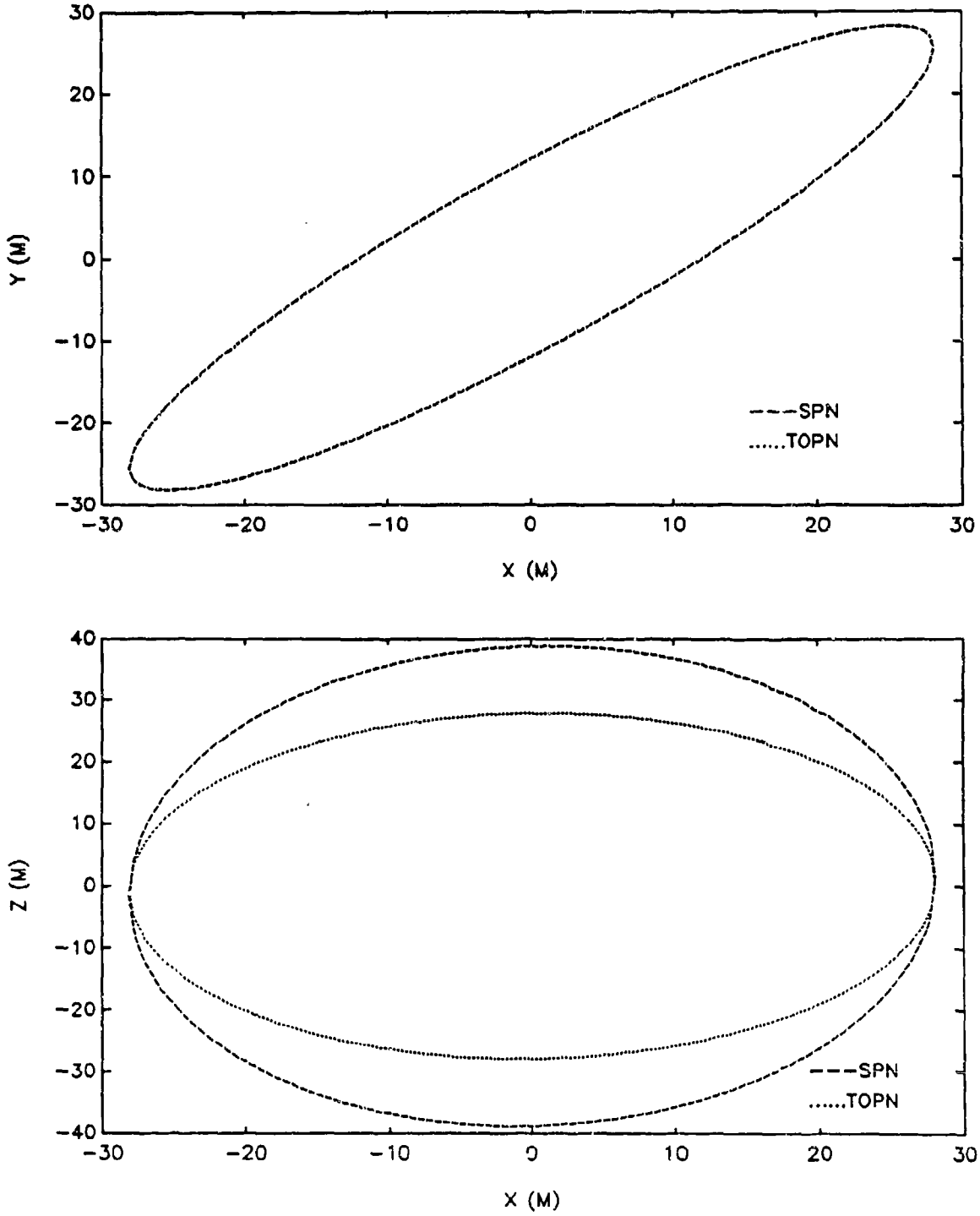

FIGURE 5-27. POSITION ERROR ELLIPSES FOR CA FILTER - TRAJ 2

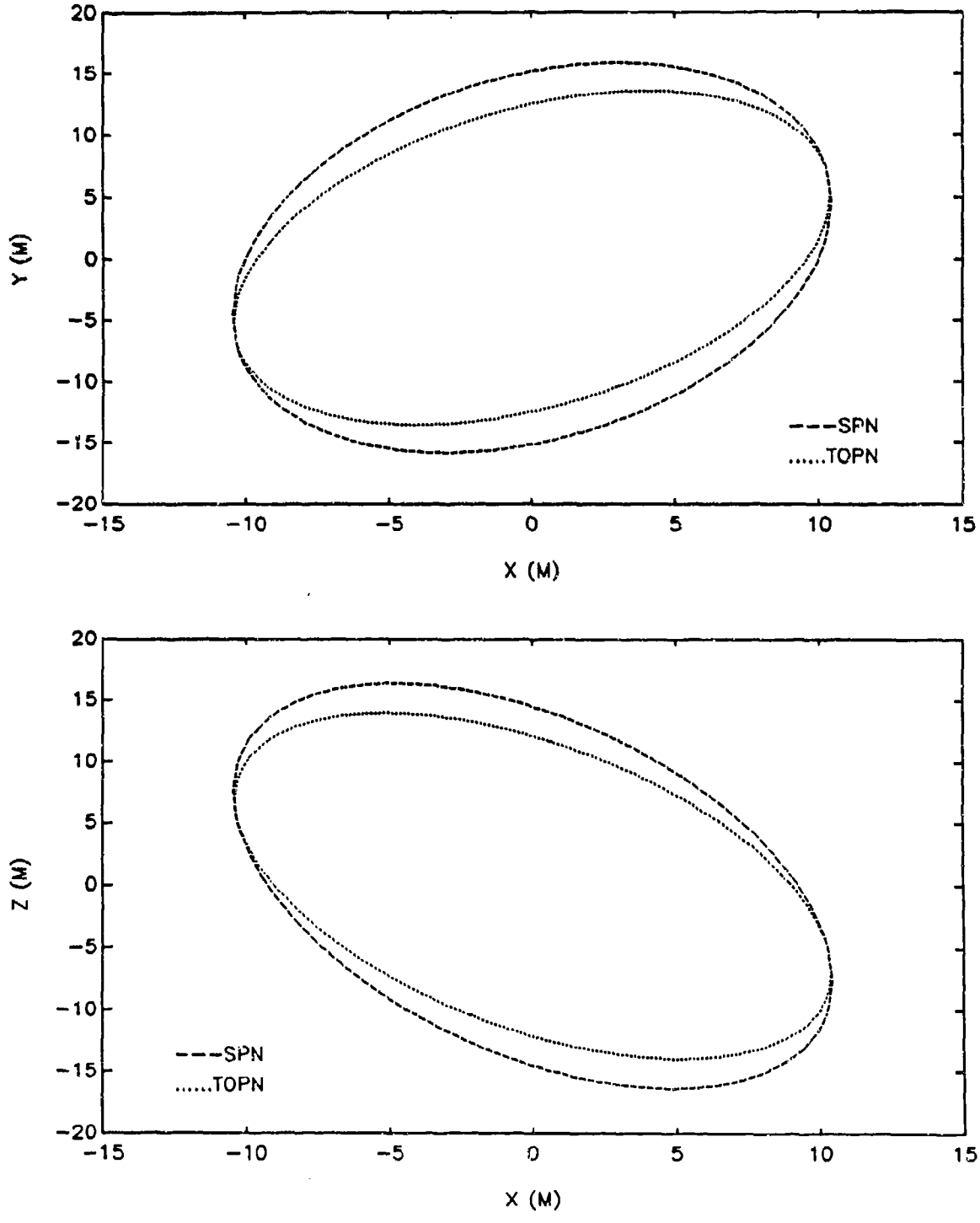

FIGURE 5-28. POSITION ERROR ELLIPSES FOR CA FILTER - TRAJ 3

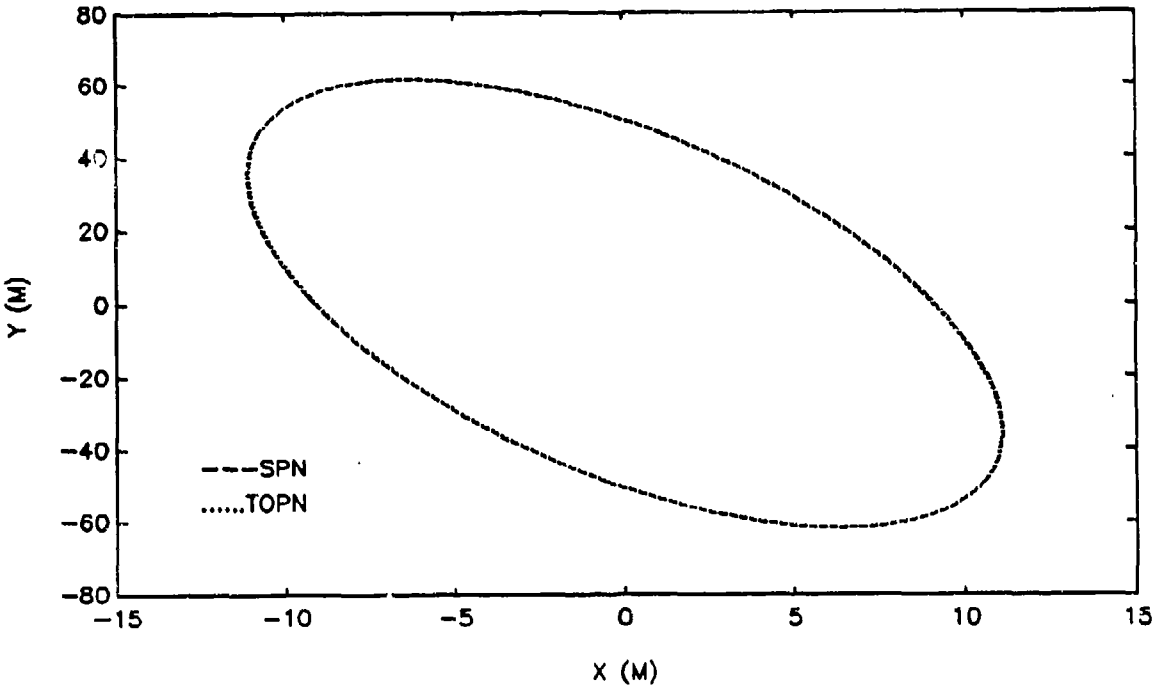

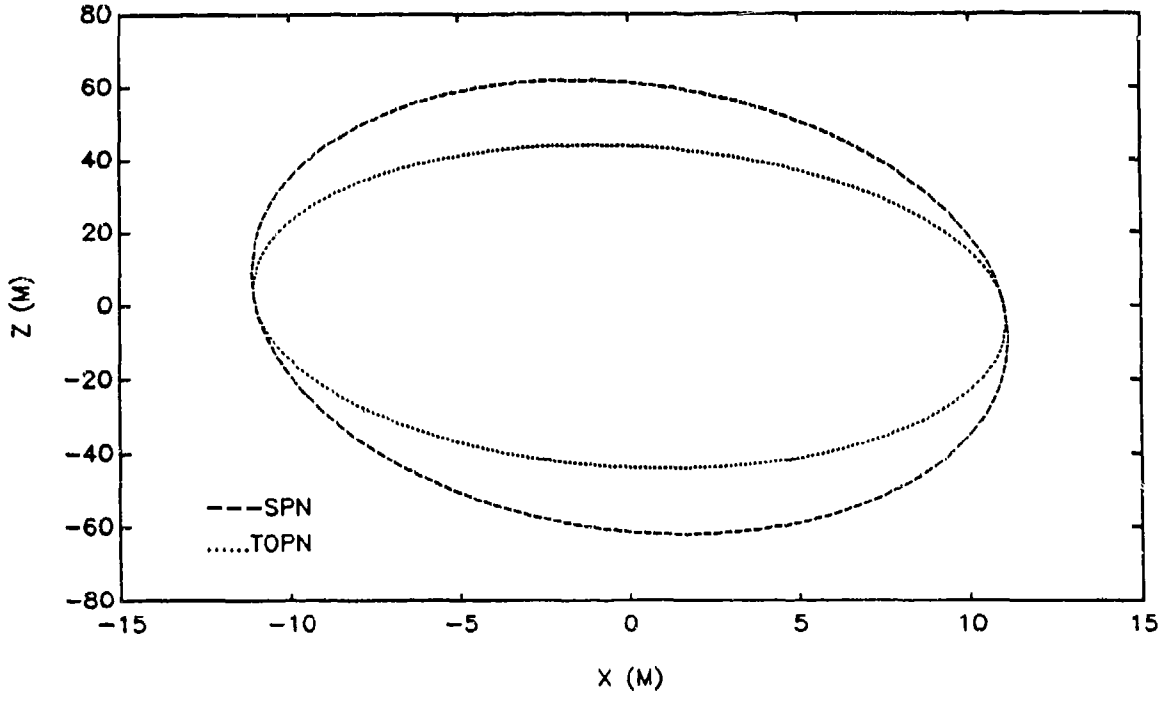

FIGURE 5-29. POSITION ERROR ELLIPSES FOR CA FILTER - TRAJ 4

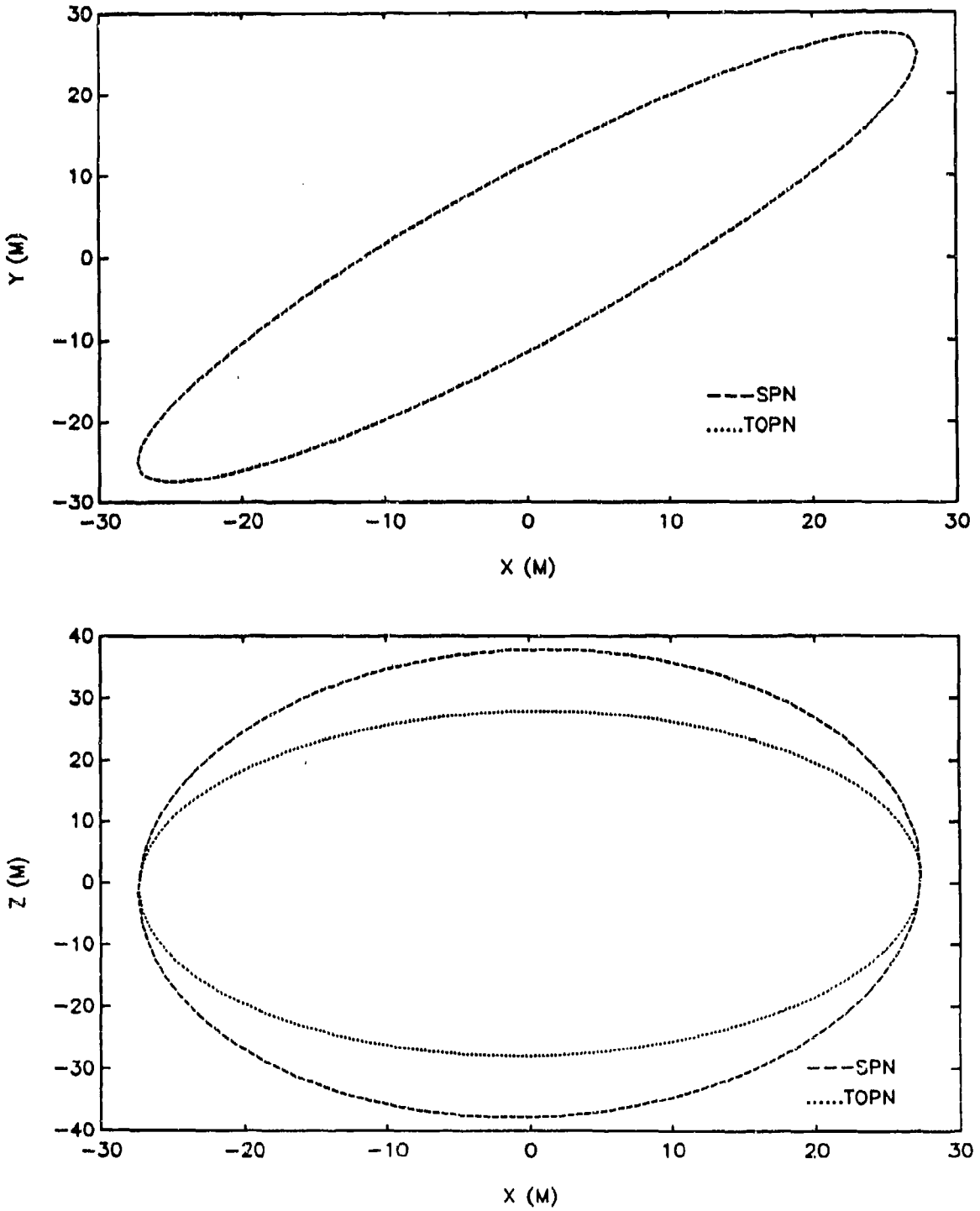

FIGURE 5-30. POSITION ERROR ELLIPSES FOR MJ FILTER - TRAJ 2

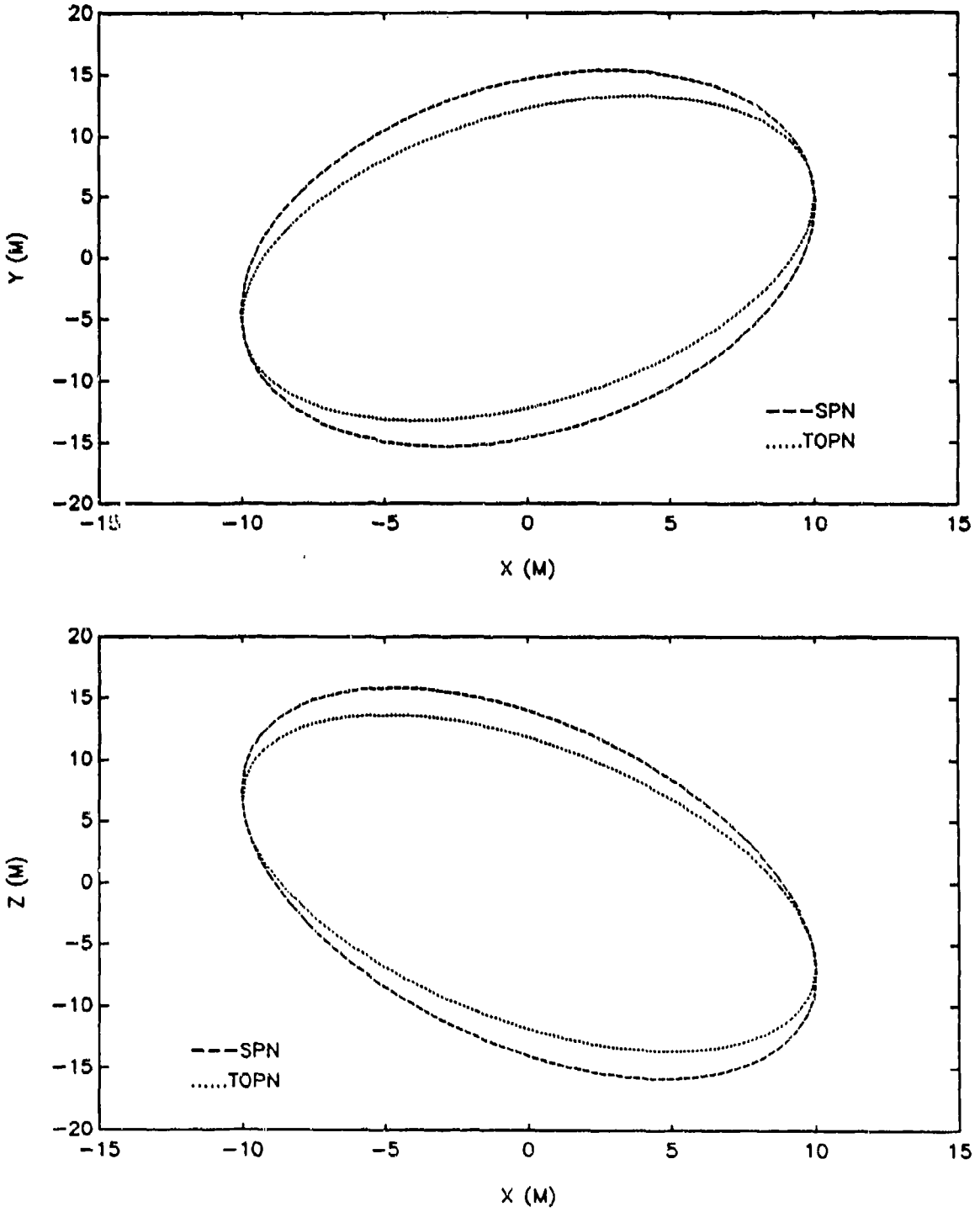

FIGURE 5-31. POSITION ERROR ELLIPSES FOR MJ FILTER - TRAJ 3

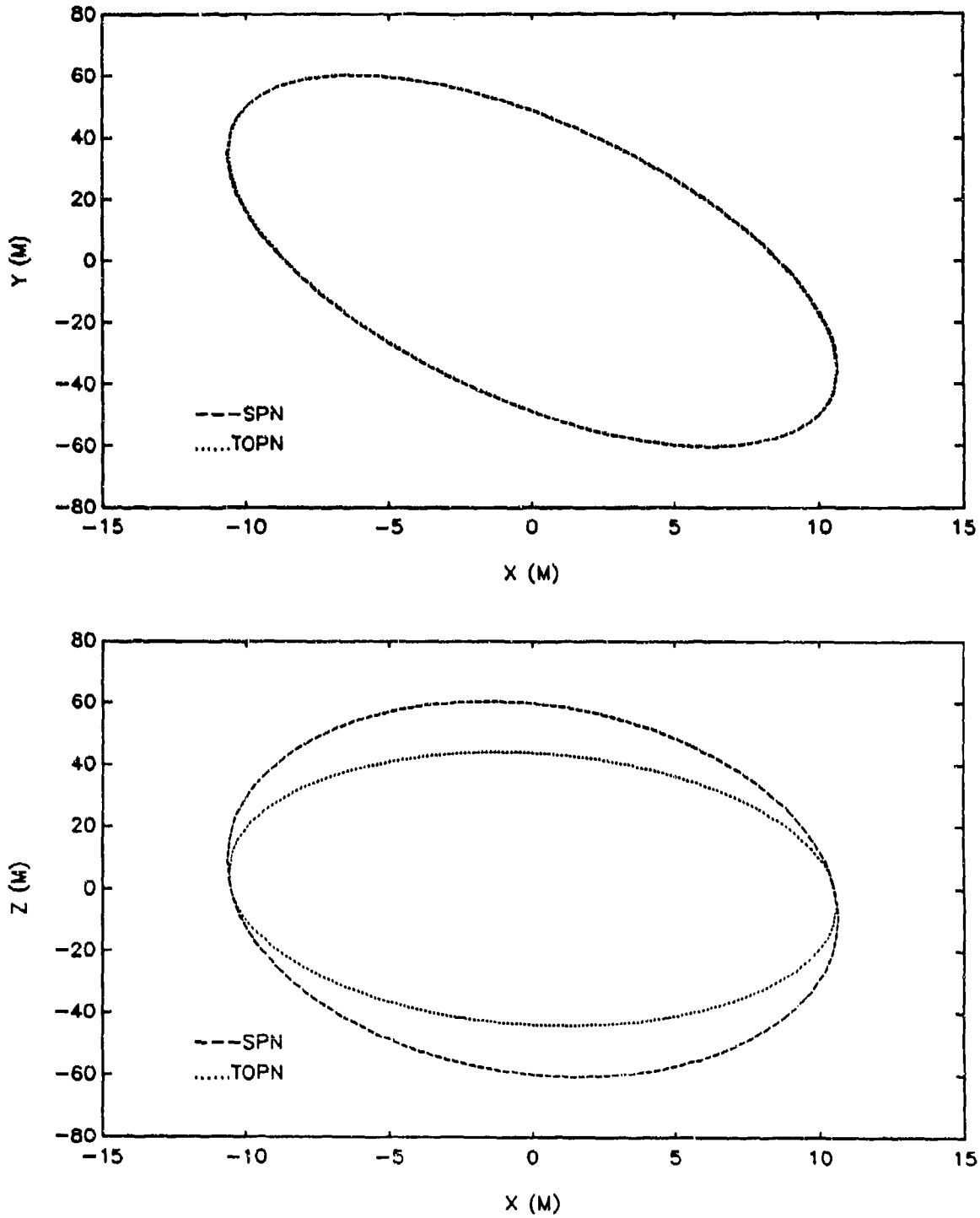

FIGURE 5-32. POSITION ERROR ELLIPSES FOR MJ FILTER - TRAJ 4

CHAPTER 6

CONCLUSIONS AND FUTURE RESEARCH

Supplementing the standard Kalman filter with a target-oriented process noise can significantly improve tracking filter performance when the target's maneuvers are confined to a plane and the filter generates an acceleration estimate so that the plane of the maneuver can be identified. The target-oriented process noise can slightly improve the tracking performance of a constant velocity filter. Adding a target-oriented process noise to a Kalman filter adds a moderate amount of computations. Therefore, its use is limited to fire control applications where only a small number of targets are tracked, and large errors in the estimates are unacceptable.

Future research may examine the more realistic situations of targets performing elaborate maneuvers in the presence of clutter and false measurements by incorporating the target-oriented process noise into algorithms such as the Interacting Multiple Model Probabilistic Data Association Filter (IMMPDAF).[10] Using a target-oriented process noise could significantly improve tracking in a cluttered environment by reducing the volume of the validation gates. Another subject for future research is supplementing a Kalman filter with both a target-oriented process noise and a kinematic constraint.[6] The kinematic constraint seems to be compatible with a target-oriented process noise since it does not affect the acceleration estimates in the direction orthogonal to the plane of motion.

CHAPTER 7

REFERENCES

1. Singer, R.A., "Estimation of Optimal Tracking Filter Performance for Manned Maneuvering Targets," IEEE Transactions on Aerospace and Electronic Systems, 1970, pp. 473-483.

2. Bar-Shalom, Y., and K. Birmiwal, "Variable Dimension Filter for Maneuvering Target Tracking," IEEE Transactions on Aerospace and Electronic Systems, Sept. 1982, pp. 621–629.

3. Clark, B.L., *Development of an Adaptive Kalman Tracking Filter and Predictor for Fire Control Applications*, NSWC TR–3445, Naval Surface Warfare Center, Dahlgren, VA, 1977.

4. Berg, R.F., "Estimation and Prediction for Maneuvering Target Trajectories," IEEE Trans. Auto. Cont., March 1983, pp. 294–304.

5. Tank, M., and J.L. Speyer, "Target Tracking Problems Subject to Kinematic Constraints," IEEE Trans. Auto. Cont., Vol. 35, No. 3, March 1990.

6. Blair, W.D., G.A. Watson, and A.T. Alouani, "Tracking Constant Speed Target Using a Kinematic Constraint," Proc. 23^{rd} Southeastern Symposium on System Theory, Columbia, SC, March 10-12, 1991.

7. Watson, G.A., and W.D. Blair, "Constant Speed Prediction Using A Three Dimensional Turning Rate," Proc. 23^{rd} Southeastern Symposium on System Theory, Columbia, SC, March 10-12, 1991.

8. Blackman, S. S., *MULTIPLE-TARGET TRACKING WITH RADAR APPLICATIONS*, ARTECH House, Inc., Norwood MA, 1986.

9. Bar-Shalom, Y. and T. Fortmann, *TRACKING AND DATA ASSOCIATION*, Academic Press, Inc., Orlando FL, 1988.

10. Houles, A. and Y. Bar-Shalom, "Multisensor Tracking of a Maneuvering Target in Clutter," IEEE Transactions on Aerospace and Electronic Systems, Vol. AES-25, No. 2, March 1989, pp. 176-189.

11. Craig, John J., *INTRODUCTION TO ROBOTICS, MECHANICS, AND CONTROL*, 1986, Addison-Wesley Publishing Company, Inc., pp. 42-44.

12. Kalata, Paul R., "The Tracking Index: A Generalized Parameter for $\alpha-\beta$ and $\alpha-\beta-\gamma$ Target Trackers," IEEE Transactions on Aerospace and Electronic Systems, Vol. AES-20, No. 2, March 1984, pp. 174-182.

APPENDIX A

DERIVATION OF ROTATION MATRIX

This appendix presents a derivation of the rotation matrix required to rotate a vector/matrix defined in the target's frame into the tracking frame. This derivation is based on the development of Z-Y-X Euler angles.[11]

A Z-Y-X Euler angles rotation matrix performs rotations about the Z, Y, and X axes in that order. The second and third rotations are performed about an axis rotated by the previous rotation; Figure A-1 illustrates these rotations.

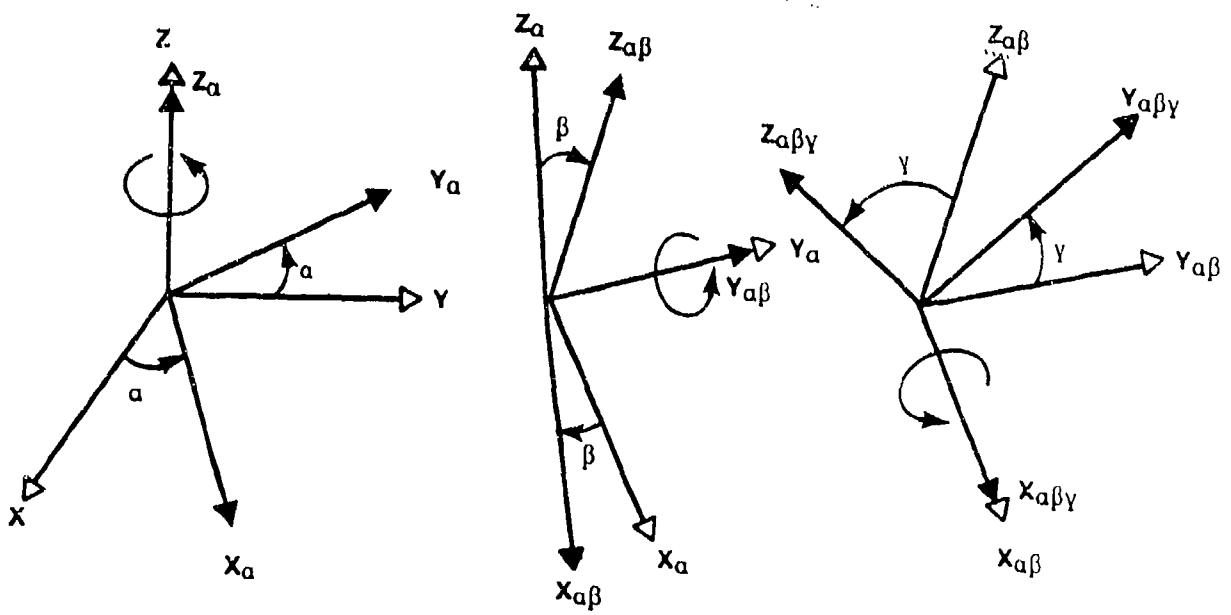

FIGURE A-1. Z-Y-X EULER ANGLES

Let ${}^A_B R_{zyx}(\alpha, \beta, \gamma)$ be a rotation matrix describing frame $\{B\}$ relative to $\{A\}$ by Z-Y-X Euler angles. This rotation matrix can be derived by viewing the rotations about $\{B\}$ axes as equivalent to negative rotations about $\{A\}$ axes. For example, rotating about $\hat{Z}_B$ by an angle α is equivalent to rotating about $\hat{Z}_A$ by an angle $-\alpha$. This leads to

$$ {}^B_A R_{zyx}(\alpha, \beta, \gamma) \quad = \quad ROT({}^B\hat{X}, -\gamma) \quad ROT({}^B\hat{Y}, -\beta) \quad ROT({}^B\hat{Z}, -\alpha) \qquad (A.1) $$

Since ${}^B_A R^{-1} = {}^A_B R$ and $ROT^{-1}(\hat{K}, -\theta) = ROT(\hat{K}, \theta)$, (A.1) becomes

$$ {}^A_B R_{zyx}(\alpha, \beta, \gamma) \quad = \quad {}^B_A R^{-1}(\alpha, \beta, \gamma) \qquad (A.2) $$

$$ = \quad ROT({}^B\hat{Z}, \alpha) \quad ROT({}^B\hat{Y}, \beta) \quad ROT({}^B\hat{X}, \gamma) \qquad (A.3) $$

$$ = \quad \begin{bmatrix} c\alpha & -s\alpha & 0 \\ s\alpha & c\alpha & 0 \\ 0 & 0 & 1 \end{bmatrix} \begin{bmatrix} c\beta & 0 & s\beta \\ 0 & 1 & 0 \\ -s\beta & 0 & c\beta \end{bmatrix} \begin{bmatrix} 1 & 0 & 0 \\ 0 & c\gamma & -s\gamma \\ 0 & s\gamma & c\gamma \end{bmatrix} \qquad (A.4) $$

$$ = \quad \begin{bmatrix} c\alpha\, c\beta & c\alpha\, s\beta\, s\gamma - s\alpha\, c\gamma & c\alpha\, s\beta\, c\gamma + s\alpha\, s\gamma \\ s\alpha\, c\beta & s\alpha\, s\beta\, s\gamma + c\alpha\, c\gamma & s\alpha\, s\beta\, c\gamma - c\alpha\, s\gamma \\ -s\beta & c\beta\, s\gamma & c\beta\, c\gamma \end{bmatrix} \qquad (A.5) $$

In Equations (A.4) and (A.5) above, 'c' and 's' are abbreviations for 'cos' and 'sin.'

The Z-Y-X Euler angles can be extracted from a given rotation matrix using the equations

$$ \alpha = \text{atan2}(r_{21}, r_{11}) \qquad (A.6) $$

$$ \beta = \text{atan2}(-r_{31}, \sqrt{r_{11}^2 + r_{21}^2}) \qquad (A.7) $$

$$ \gamma = \text{atan2}(r_{32}, r_{33}) \qquad (A.8) $$

where the r_{ij} are unit vector elements of some matrix defining the orientation of frame B with respect to frame A. Note: atan2 is the two-argument arc tangent function (also called the 4-quadrant arc tangent function). Notice that the equations are valid only when $\beta \neq \pm 90$ degrees. When this situation occurs, α is set to zero and γ is then computed from the equations

$$ \gamma = \quad \text{atan2}(r_{12}, r_{22}) \qquad (A.9) $$

if $\beta = 90$ and

$$ \gamma = \quad -\text{atan2}(r_{12}, r_{22}) \qquad (A.10) $$

if $\beta = -90$.

The rotation matrix given in Equation (4.4) for a constant velocity filter was derived from the one given in Equation (4.2), as follows. The rotation matrix given in Equation

(4.2) can be computed from Z-Y-X Euler angles by using Equations (A.6), (A.7), and (A.8) which gives

$$\alpha = \text{atan2}(\frac{\dot{y}}{Sh}, \frac{\dot{x}}{Sh}) \tag{A.11}$$

$$\beta = \text{atan2}(\frac{-\dot{z}}{S}, \frac{Sh}{S}) \tag{A.12}$$

$$\gamma = \text{atan2}\Big(\frac{\bar{z}^l}{|A_k^l|}, \frac{\dot{x}\bar{y}^l - \bar{x}^l\dot{y}}{S|A_k^l|}\Big) \tag{A.13}$$

where $S = |V_k| = (\dot{x}_k^2 + \dot{y}_k^2 + \dot{z}_k^2)^{\frac{1}{2}}$, $Sh = (\dot{x}_k^2 + \dot{y}_k^2)^{\frac{1}{2}}$, and $|A_k^l|$ is the magnitude of the lateral acceleration vector. Notice that an acceleration estimate is required to compute γ in Equation (A.13), and a constant velocity filter does not generate an acceleration estimate. Thus, γ in the general rotation matrix form given in Equation (A.5) is set to zero which gives

$$\overset{A}{B}R_{zyx}(\alpha, \beta) = \begin{bmatrix} c\alpha\, c\beta & -s\alpha & c\alpha\, s\beta \\ s\alpha\, c\beta & c\alpha & s\alpha\, s\beta \\ -s\beta & 0 & c\beta \end{bmatrix} \tag{A.14}$$

where B denotes the target's frame and A denotes the sensor's frame. Then Equation (4.4) is obtained by replacing $c\alpha$, $s\alpha$, $c\beta$, and $s\beta$ in Equation (A.14) with their equivalents found from Equations (A.11) and (A.12).

APPENDIX B

ERROR ELLIPSE PLOTTING ALGORITHM

This appendix presents the algorithm used to plot the position error ellipses. To obtain an equation for a position error ellipse in the horizontal plane from the filtered error covariance matrix, the following equation is expanded

$$[X \quad Y]\begin{bmatrix} \sigma_X^2 & \sigma_X\sigma_Y \\ \sigma_X\sigma_Y & \sigma_Y^2 \end{bmatrix}\begin{bmatrix} X \\ Y \end{bmatrix} = c_1 \qquad (B.1)$$

where X and Y are the position states in Cartesian coordinates, σ_X^2 and σ_Y^2 are the filtered error variances of the corresponding position states which are extracted from the filtered error covariance matrix, and c_1 is a constant whose value is found from a Chi-squared table. The value chosen for c_1 determines the confidence region. For the plots shown in Figures 5-26 through 5-32, c_1 was chosen to be 2.5 which produced ellipses defining the 99% confidence region. Equation (B.1) can be expanded to the form

$$\frac{X^2}{\sigma_X^2} - \frac{2\rho XY}{\sigma_X\sigma_Y} + \frac{Y^2}{\sigma_Y^2} = (1-\rho^2)c_1 \qquad (B.2)$$

where $\rho = \dfrac{\sigma_{XY}^2}{\sigma_X\sigma_Y}$ is the correlation coefficient. Using the quadratic formula to solve Equation (B.2) gives

$$Y = \frac{-b \pm \sqrt{b^2 - 4ac_2}}{2a} \qquad (B.3)$$

where $a = \dfrac{1}{\sigma_Y^2}$, $b = \dfrac{-2\rho X}{\sigma_X\sigma_Y}$, and $c_2 = \dfrac{X^2}{\sigma_X^2} - c_1(1-\rho^2)$.

The horizontal position ellipse is obtained by plotting Y of Equation (B.3) for values of X in the region defined by

$$-\sqrt{c_1\sigma_X^2} \le X \le +\sqrt{c_1\sigma_X^2} \qquad (B.4)$$

To obtain the position error ellipse in the vertical plane, replace Y in Equation (B.3) by Z and replace σ_Y^2 by σ_Z^2.

DISTRIBUTION

	Copies
CENTER FOR NAVAL ANALYSES 4401 FORD AVE ALEXANDRIA VA 22302-0268	1
DEFENSE TECHNICAL INFORMATION CENTER CAMERON STATION ALEXANDRIA VA 22304-6145	12
ATTN DR RABINDER MADAN 114SE CHIEF OF NAVAL RESEARCH 800 NORTH QUINCY ST ARLINGTON VA 22217-5000	1
ATTN DR GLENN M SPARKS GOVERNMENT ELECTRONIC SYSTEMS DIVISION GENERAL ELECTRIC COMPANY MOORESTOWN NJ 08057	1
ATTN PROF YAAKOV BAR-SALOAM ESE DEPARTMENT U-157 260 GLENBROOK RD STORRS CT 06268-3157	1
ATTN A T ALOUANI DEPARTMENT OF ELECTRICAL ENGINEERING TTU BOX 05004 TENNESSEE TECHNOLOGICAL UNIVERSITY COOKEVILLE TN 38505	1
ATTN GIFT AND EXCHANGE DIVISION LIBRARY OF CONGRESS WASHINGTON DC 20540	4
ATTN P K RAJAN DEPARTMENT OF ELECTRICAL ENGINEERING TTU BOX 05004 TENNESSE TECHNOLOGICAL UNIVERSITY COOKEVILLE TN 38505	1
ATTN EDWARD PRICE FMC CORPORATION 1 DANUBE DR KING GEORGE VA 22485	1
ATTN SCOTT GODFREY FMC CORPORATION 1 DANUBE DR KING GEORGE VA 22485	1
ATTN DR RAGHAVAN LNK CORPORATION 6800 KENILWORTH AVE SUITE 306 RIVERDALE MD 20737	1
ATTN GLENN WOODARD SYSCON CORPORATION TIDEWATER DIVISION PO BOX 1480 DAHLGREN VA 22448-1480	1

DISTRIBUTION (Continued)

	Copies
INTERNAL DISTRIBUTION	
E231	3
E232	2
E261 WAITS	1
E32 GIDEP	1
F1	1
F20	1
F21	1
F21 PARKER	10
F21 BLANKENSHIP	1
F41 TANNER	1
F41 MARTIN	1
F44	1
G	1
G05	1
G06	1
G07	1
G11 DOSSETT	1
G11 GROVES	1
G11 LUCAS	1
G13 BEUGLASS	1
G20	1
G23 OHLMEYER	1
G23 JOHN BIBEL	1
G23 MALYEVAC	1
G70	1
G702 AUGER	1
G706 BUSCH	1
G71	1
G71 BLAIR	10
G71 RICE	1
G71 J. GRAY	1
G71 MURRAY	1
G71 J. CONTE	1
G72 GENTRY	1
G72 BOYKIN	1
G73 FONTANA	1
N05	1
N05 GASTON	1
N24	1
N24 BAILEY	1
N24 HANSEN	1
N35 BOYER	1
N35 HELMICH	1
N35 HARTER	1
N35 BAILEY	1
N35 FENNEMORE	1

REPORT DOCUMENTATION PAGE

Form Approved
OMB No. 0704-0188

1. AGENCY USE ONLY *(Leave blank)*	2. REPORT DATE	3. REPORT TYPE AND DATES COVERED
	August 1992	

4. TITLE AND SUBTITLE
Use of Target-Oriented Process Noise in Tracking Maneuvering Targets

5. FUNDING NUMBERS

6. AUTHOR(S)
J. Darren Parker W. D. Blair

7. PERFORMING ORGANIZATION NAME(S) AND ADDRESS(ES)
Naval Surface Warfare Center
Dahlgren Division (Code F21)
Dahlgren, VA 22448-5000

8. PERFORMING ORGANIZATION REPORT NUMBER
NAVSWC TR 91-701

9. SPONSORING/MONITORING AGENCY NAME(S) AND

10. SPONSORING/MONITORING AGENCY REPORT NUMBER

11. SUPPLEMENTARY NOTES

12a. DISTRIBUTION/AVAILABILITY
Approved for public release; distribution is unlimited.

12b. DISTRIBUTION CODE

13. ABSTRACT *(Maximum 200 words)*

Kalman filters for target tracking typically use a process noise defined in the tracking frame. This requires setting the variances of the process noise in all three Cartesian coordinates to values large enough to compensate for the largest possible target maneuver. This report investigates the performance of a Kalman filter that uses a target-oriented process noise. A target-oriented process noise is obtained by rotating a process noise, defined in the target's frame, into the tracking frame. The rotation matrix is computed from the state estimates of the Kalman filter.

The results of Monte Carlo simulations are presented that demonstrate that a Kalman filter with a target-oriented process noise tracks coordinated turning targets with smaller root-mean-square (RMS) errors than a Kalman filter with standard process noise. It was determined that if the target-oriented process noise is to be effective, the Kalman filter must generate an acceleration estimate, and the target's maneuver should be confined to a plane.

14. SUBJECT TERMS			15. NUMBER OF PAGES
Kalman Filter	Target	Tracking	72
Target-OrientedProcess Noise	Process Noise	Monte Carlo simulations	16. PRICE CODE

17. SECURITY CLASSIFICATION OF REPORT	18. SECURITY CLASSIFICATION OF THIS PAGE	19. SECURITY CLASSIFICATION OF ABSTRACT	20. LIMITATION OF ABSTRACT
UNCLASSIFIED	UNCLASSIFIED	UNCLASSIFIED	SAR